buildings

MDPI

*Article*

# Cyclic Behavior of the Column-Tree Moment Connection with Weakened Plates: A Numerical Approach

**Pablo Matthews and Eduardo Núñez ***

Department of Civil Engineering, Universidad Católica de la Santísima Concepción, Concepción 4070128, Chile; pablo.matthews@ucsc.cl
* Correspondence: enunez@ucsc.cl

**Abstract:** The use of column-tree connections is common in controlled shop environments due to their cost-effectiveness in achieving ductile welds. Field bolts are also easy to install and inspect. However, there is currently no prequalification available for these connections, their performance is not fully understood, and the cost of aftermath repairs is still a major concern for owners. In this research, analytical and numerical studies were performed to assess the cyclic behavior considering the effects of the bolted splice location, bolt slippage, and splice plate thickness. Fourteen numerical models using the finite element method in ANSYS software were analyzed to evaluate the nonlinear behavior of moment connection configurations in terms of the strength, stiffness, ductility, energy dissipation, and overall cyclic response. The results showed that appropriately proportioned bolted splice connections can meet the requirements for prequalified moment connections. The models complied with the criteria established in AISC 358 and achieved flexural resistance that was higher than 80% of the beam plastic moment at 4% of the interstory drift ratio. The weakened plates concentrated the inelastic action, which allowed us to prevent the brittle behavior and damage to the column, welding, and other components of the moment connection. Complex geometries or specially fabricated parts were not required, providing a cost-effective way to control seismic-related damage. Also, required repairs are based on the replacement of standard parts, reducing operational detentions in facilities. Finally, the moment connection studied is classified as partially restrained (PR) according to the requirements established in AISC 360.

**Keywords:** steel moment connection; plates; cyclic behavior; bolted connections; finite elements

check for updates

**Citation:** Matthews, P.; Núñez, E. Cyclic Behavior of the Column-Tree Moment Connection with Weakened Plates: A Numerical Approach. *Buildings* **2023**, *13*, 2908. https://doi.org/10.3390/buildings13122908

Academic Editors: Hai-Ting Li, Fangxin Hu and Shujun Hu

Received: 25 September 2023
Revised: 16 October 2023
Accepted: 24 October 2023
Published: 22 November 2023

**Copyright:** © 2023 by the authors. Licensee MDPI, Basel, Switzerland. This article is an open access article distributed under the terms and conditions of the Creative Commons Attribution (CC BY) license (https://creativecommons.org/licenses/by/4.0/).

## 1. Introduction

Steel moment frames are well-known for their ability to withstand intense seismic events by absorbing energy. However, the ductility of these frames mainly depends on the performance of their connections, which can be either fully or partially restrained [1]. These connections are where the maximum moment demand occurs.

In 1994, the Northridge Earthquake caused unexpected and severe damage to these moment frame connections. The typical connection configuration at the time was a wide flange rolled beam site welded directly to a wide flange column, and this event prompted a closer look at ductility-related issues such as the welding details and material toughness [1]. The findings of the investigation revealed brittle fractures around the welds, leading to improvements in welding technologies and the standardization of prequalified connections [2].

In 1995, the Kobe Earthquake revealed that steel moment frames had similar failures to those seen in previous earthquakes [3]. In this case, the use of welded or cold-formed box-columns or cross-shaped columns was observed. Additionally, instead of site-welded beams, the column typically had shop-welded beam stubs, and the main beam was field-bolted. This design is referred to as "column-tree" [4]. Although the shop-welded connection has better conditions for achieving strong welds and related inspections, there

were still instances of brittle fractures at the welds. According to Whittaker [5], "Japanese framing systems tend to be more redundant than similar systems in the US".

Research efforts were then dedicated to enhancing the technology of welding consumables, as well as improving the material toughness and joint preparation geometry [6]. The significance of proper ductile welds at the joint is underscored by these two seismic events. One strategy to achieve this is to reinforce the welding area and provide a greater cross-section, thereby reducing tensile stresses at the welds. Chen et al. [7] examined the impact of widened beam flange specimens, while Kang et al. [8] introduced external stiffeners at the connection with HSS columns. This design philosophy enhances the overall ductility, but brittle weld fractures may still occur during the final load cycles. Schneider and Teeraparbwong [9] tested connections with bolted flange cover plates of varying bolt geometries and quantities, resulting in a high rotational capacity and typically forming the girder hinge near the cover plates.

An alternative method is to relocate the area where the inelastic action occurs from the welded joints and instead place it in the steel beam [10]. One approach to achieving this is by designing a reduced beam section (RBS) [2], which moves the plastic hinge away from the column face. Researchers like Zhang et al. [11], Morshedi et al. [12], and Vetr et al. [13] explored different designs such as beams with openings at the web, double-RBS beams, and beams with drilled holes of various diameters at the beam flanges. By deliberately weakening a specific section of the beam, a ductile mechanism can be predicted and controlled for high cycle loads.

There are various ways to configure structures using different concepts. One example is the end-plate connection, which is explained in AISC 358 [2]. This type of connection involves plates that are prewelded in the shop, sometimes with stiffeners. In a study by Nuñez et al. [14], the seismic performance of end-plate moment connections on HSS columns was analyzed. The test results showed a maximum reaction of 1.9 Mp at 4% rad drift. Tao et al. [15] also conducted tests on end-plate connections that were applied to concrete-filled HSS columns, where the bolts passed through the entire column section.

While all of these moment connection improvements effectively resolve previous brittle performance challenges (like weld cracking, beam buckling, or beam fracture), the problem of connection ductile damage still lingers as an economic setback for building owners and industrial facilities that must detain operations if complex repair activity is required. This challenge invites us to revisit the column-tree connection as a possible solution to find a cost-effective way to limit ductile damage and repair costs.

In a comprehensive examination conducted by Astaneh-Asl [16], the focus was on the connections between column-trees, considering a variety of factors, including the number and size of bolts, the thickness of the connection plate, and the distance from the column. The objectives were to avoid any potential for brittle failure mechanisms and to enhance the structure's seismic performance by creating a balanced connection design that could act as a fuse to minimize seismic forces.

In a study conducted by Baharamast et al. [17], various iterations of bolted column-tree connections were explored, including reinforcements and reduced sections. Similarly, Gharebaghi and Hosseini [18] investigated the impacts of bolt pretension and clearance. However, both studies utilized a fully rigid splice that did not incorporate connection plates for energy dissipation. Alternatively, Palizzolo and Vazzano [19] and Chen et al. [20] proposed specially fabricated connection devices that concentrated energy dissipation through plastic strain or friction. These devices had the added benefit of being replaceable after a severe earthquake. In New Zealand, Yeow [21] examined the advantages and drawbacks of utilizing friction connections to decrease the expenses and repair time after earthquakes.

Oh et al. [22] conducted a study on the performance of three column-tree specimens, each with different plate thicknesses and bolt quantities, under the AISC 341 [23] qualification loading protocol. The connections were designed to have a strength of 95% of the beam plastic moment Mp for several intended failure mechanisms: bolt slip (CT), bolt

bearing (CT-B), and plate yielding (CT-R). The test results indicated that the typical failure mode was beam flange local buckling, with ultimate strengths ranging from 1.3 Mp to 1.5 Mp and a higher level of energy dissipation when compared to fully rigid connections. Specimen CT-R, which had fewer bolts, experienced early bolt slip that prevented significant yielding of the splice plates. This suggests that energy dissipation occurred through friction and plastic strain, which are complementary. Furthermore, Oh et al. [24] compared the responses of composite and noncomposite column-tree connections and found that the presence of a concrete slab reduced the system's ductility.

In a study conducted by Lin et al. [25], it was discovered that the design strength can be represented by Md = FCR × My, where FCR is a parameter that ranges from 0.85 to 0.95 to account for a decreased required strength at a connection situated away from the column. In this equation, $My = S_x \times Fy$ is used in place of $Mp = Z_x \times Fy$. The connection plates are designed to function as replaceable damage-control fuses, following the RBS philosophy. The study's results successfully showed that the plastic strain is concentrated at the splice plates, which decreases damage to the beam and column. Karami et al. [26] expanded on Oh's [22] research by using numerical nonlinear models to add three instances where the reduced strength connection type CT-R was located at various distances from the column. The findings revealed that the connection's ultimate strength is not affected by its position. However, as the distance increases, the connection becomes less effective at dissipating energy and reduces the weld. The main objective of this report was to determine if a connection could be prequalified for SMRFs. The results indicate that it is achievable, but it depends on the location and stiffness of the bolted splice. A connection located near the column and/or with a weakened splice will be classified as semi-rigid and cannot be used as a prequalified connection in the SMRF.

The engineering community does not have a complete understanding of the seismic performance of bolted column-tree connections. The response can be affected by variables such as the location, bolt configuration, and plate thickness. Following the Kobe Earthquake in 1995, doubts were raised about the design of fully rigid bolted connections, and a more ductile response was favored. Previous research is very clear regarding the ductility of a weakened bolted splice: the connection plates are a very good source of energy dissipation through plastic strain and plate friction [27]. However, their use in SMRFs worldwide is limited due to the lack of a straightforward design procedure that can predict the connection's cyclic behavior and ensure compliance with seismic requirements.

Another interesting aspect of designing weakened splices is the concentration of plastic strain after a severe earthquake, which protects the beam and column from damage. The behavior of bolted steel plates under fire conditions has also been studied by Akagwu et al. [28]; Yeow et al. [21] demonstrated that replacing damaged plates and bolts is a cost-effective way to repair the connection and reduce time and labor. Saravanan et al. [29] reviewed this approach of replaceable fuses and highlighted the need for further research in this area.

The characterization of the cyclic behavior of column-tree moment connections has not been completely developed, and the use of cover plates as fuse components in the connection has not been studied. The goal of this research is to assess the cyclic behavior of the bolted splice connection, considering the cover plates as fusible components. Therefore, beams and columns are protected. Additionally, the failure mechanisms used to define the nonlinear response of the column-tree moment connection are obtained. In this sense, the influences of the beam stub length, number of bolts, and plate thickness on the cyclic response, with a particular focus on the dissipation in the beam plates as the primary failure mechanism, are developed. Posteriorly, a design procedure considering the failure mechanisms of the connection is proposed. Robust numerical models using the finite element method (FEM) are used to evaluate the cyclic response in terms of the strength, ductility, and energy dissipation capacity. Finally, this conceptualization of the column-tree moment connection allows us to achieve a cost-effective replacement with lower detention times for the facilities.

## 2. Analytical Study

According to research conducted by Astaneh-Asl [16], prioritizing ductile failure modes over brittle ones is crucial. This philosophy must be integrated into the design process with the key parameters highlighted in Figure 1. The single splice cover plates carry both tension and compression forces, while the flange bolts are pretensioned to provide initial strength against the relative slip of the flange plates.

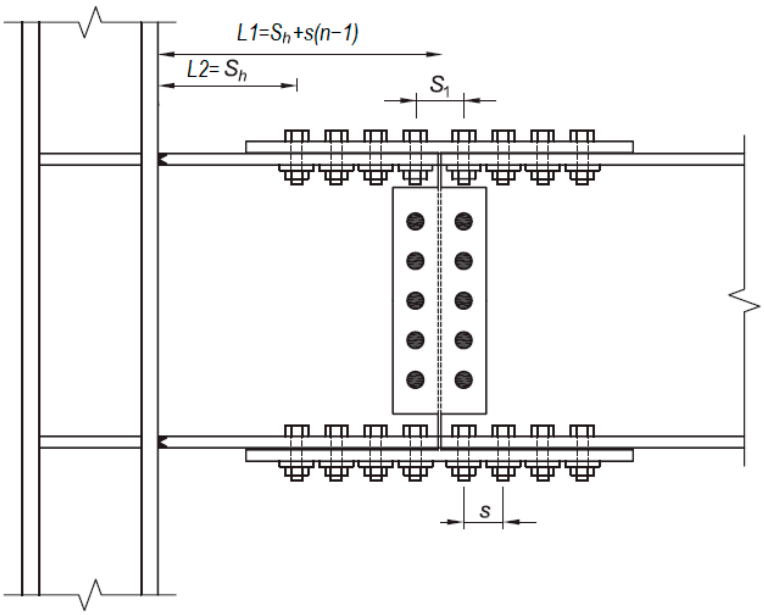



**Figure 1.** Details of the column-tree moment connection.

To achieve the goal of this study, is necessary to decrease the tensile stress in the welds between the beam stub and the column face using splice plates as a damage-control fuse. Therefore, any prequalified joint preparation for complete penetration welds is suitable, requiring no further discussion. However, for a typical moment frame that experiences lateral forces, there is a lineal moment distribution along the beam, with a maximum value at the column joint and a value near zero at the center of the span for seismic forces (as shown in Figure 2). Thus, the location of the bolted splice directly affects the required strength for the splice. Astaneh-Asl [16] recommends a distance for the splice in the range of 1/10 to 1/8 of the span.

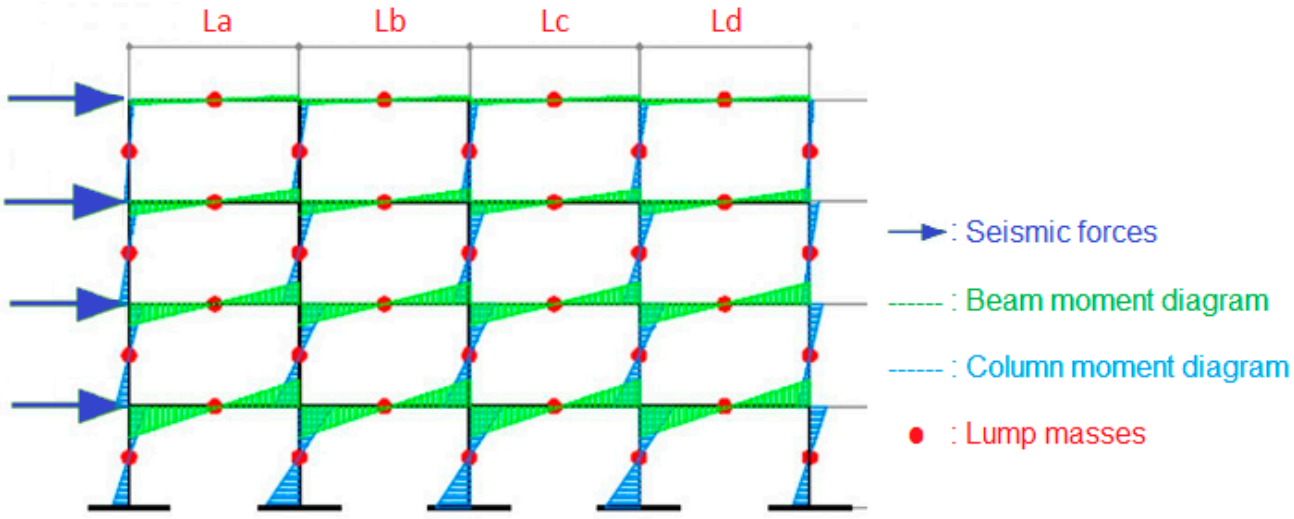



**Figure 2.** Distribution of seismic forces in steel moment frames.

The moment diagram factor "$f$" for typical frames ranges from 0.75 to 0.80. However, for atypical cases, this value may range from 0.60 to 0.85 of this value. A simple formulation can be used to consider this effect.

$$f = \left(1 - 2 * \frac{L_1}{L}\right) \tag{1}$$

where "$L_1$" is the beam stub length and "$L$" is the beam clear span.

The required splice strength "Mps" is calculated based on the moment diagram factor "f" and the following material properties:

$$\begin{array}{cc} \text{beam yielding strength} & \text{Fyb} \\ \text{splice plate yielding strength} & \text{Fys} \\ \text{beam elastic module} & \text{Sxb.} \\ \text{splice plastic module} & \text{Zxs} \\ \text{beam elastic moment strength} & \text{Myb} = \text{Fyb} \times \text{Sxb} \end{array} \tag{2}$$

$$\text{splice plastic moment strength} \quad \text{Mps} = \text{Fys} \times \text{Zxs}, \tag{3}$$

$$\text{splice design condition} \quad \text{Mps} > \text{f} \times \text{Myb} \tag{4}$$

$$\text{splice design condition} \quad \text{Zxs} > \text{f} \times \text{Sxb} \times \text{Fyb/Fys} \tag{5}$$

Moreover, the maximum size of the bolts must be determined, and then the minimum bolt quantity must be obtained. The bolt size and corresponding standard hole size affect the failure mode of the drilled beam flange and splice plates. To ensure a ductile response, the maximum bolt size depends on the beam flange geometry and material properties. We followed the AISC 360 [30] recommendations for expected yielding and expected tensile fracture at the beam flange gross area "Agf" and beam flange net area "An". Sufficient spacing between bolts must be provided to avoid block shear tear-out.

$$\text{The yielding strength is obtained as} \quad \text{Rny} = \text{Ry} \times \text{Agf} \times \text{Fyb}. \tag{6}$$

$$\text{The fracture strength is estimated as} \quad \text{Rnu} = \text{Ru} \times \text{Anf} \times \text{Fub}. \tag{7}$$

For two (2) lines of bolts across the beam flange, the net section is the

$$\text{beam flange net area} \quad \text{Ans} = \text{tf} \times (\text{B} - 2 \times \text{dh}) \tag{8}$$

where tf is the beam flange thickness, B is the beam flange width, "dh" is the bolt hole size (diameter), and the ductile mode is achieved if Rnu > Rny; therefore

$$\text{dh} < \text{B}/2 \times (1 - (\text{Ry} \times \text{Fyb})/(\text{Rt} \times \text{Fub})) - 2\,\text{mm}. \tag{9}$$

The minimum quantity of bolts is calculated based on the bearing strength; however, the slip strength must be checked, since its value is roughly 55–85% of the bolt shear strength (depending on the surface friction coefficient). To avoid the occurrence of slippage too early with low cycle loads, a great number of bolts is desirable, but avoiding slippage at all must not be pursued, since the connection would lose its energy dissipation capacity.

$$\text{required tension at the shear plane} \quad \text{Tr} = \text{Mps/d} \tag{10}$$

$$\text{required flange bolts} \quad \text{N} > \text{Tr}/0.75 \times \text{Fn} \times \text{Ab} \tag{11}$$

$$\text{slip strength} \qquad Rs = 1.13 \times \mu \times Tb \tag{12}$$

where d is the beam height, Fn is the bolt nominal shear stress, Ab is the gross area of the bolt, Tb is the bolt pretension, and μ is the mean slip coefficient. A proper and representative slip factor has to be used. Then, the overall slip strength for the group of bolts should be 50–85% of the splice plate yielding strength to provide energy dissipation during medium-range load cycles [16].

The plate thickness must fulfill the same requirements as the beam flange regarding the net area and minimum bolt pitch in order to avoid brittle modes. Special attention should be paid to the distance S1 and the plate compression buckling strength (with K = 0.5 for a continuous plate)

$$\text{radius of gyration} \qquad r = e \times \sqrt{12} \qquad \text{for a rectangular plate} \tag{13}$$

$$\text{plate slenderness} \qquad \lambda = K \times S1/r \tag{14}$$

$$\text{plate slenderness} \qquad \lambda = \sqrt{12} \times S1/e = 3.5 \times S1/e \tag{15}$$

As Lin et al. [25] suggested a maximum slenderness of 35, it has been established a "rule of thumb" for the minimum plate thickness as e > S1/10.

Finally, the gap between the beam stub and the link beam must provide enough clearance to avoid the clash of both members, affecting the plastic response of the connection and damaging the parts. As shown in Figure 3, the minimum gap is $\varnothing_U = 2 \times \delta_0/h$. Since the target rotation is at least 0.04 rad for ductile frames, the minimum gap is

$$\delta_0 = \varnothing_U * h/2 > 0.02 \times h = h/50 \tag{16}$$

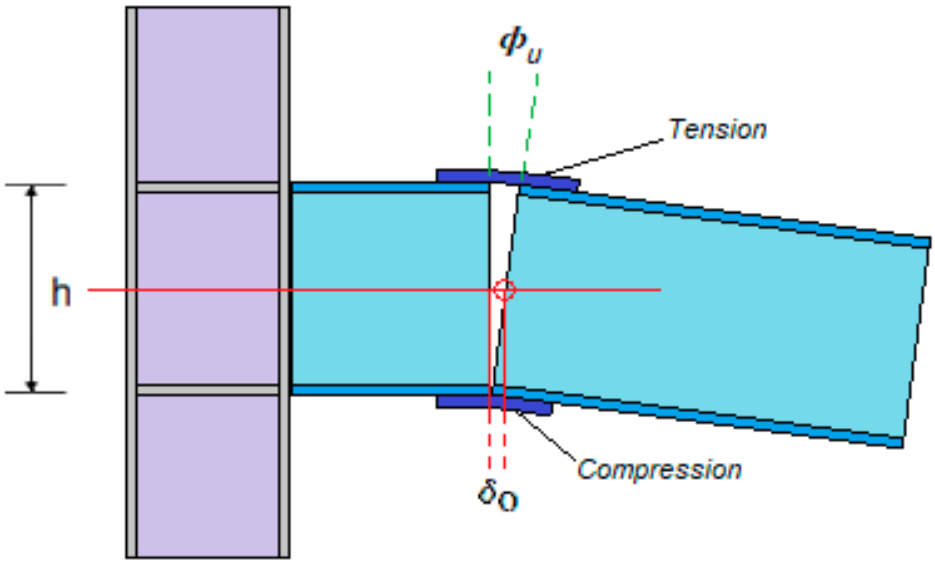



**Figure 3.** Relationship between the connection rotation, beam height, and required separation.

## 3. Numerical Study

The numerical study was based on the modeling of beam–column joint configurations in their test specimen condition (see Figure 4), which will be reported in a future article. The modeling and analysis were performed using finite elements by means of ANSYS software v2022 [31]. An explicit model of the elements was used. The elements and components of the connection were modeled explicitly. The materials used were introduced as input variables from the constitutive law of the material, while the load was considered from the application of cyclic displacements, as established by AISC 341 [23].

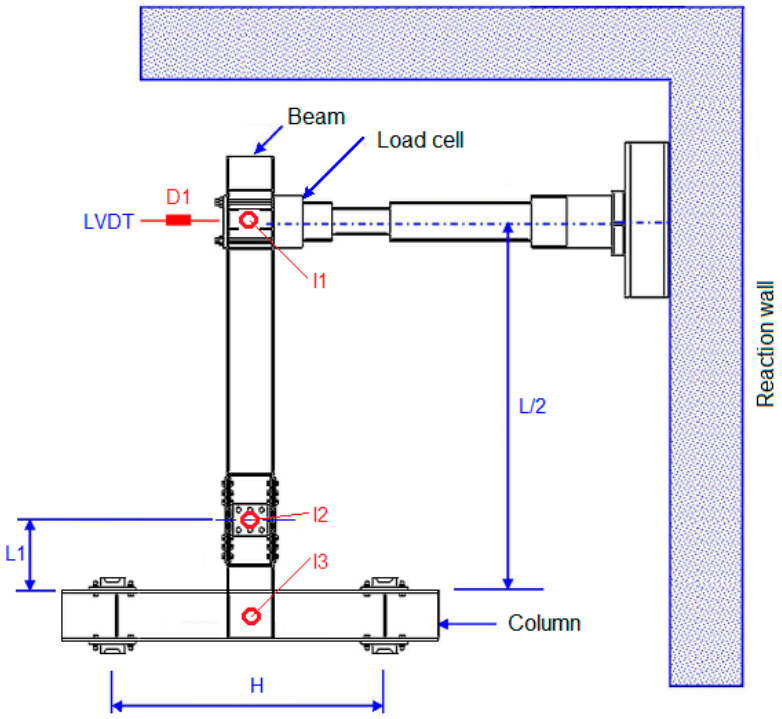



**Figure 4.** Representation of the test assembly.

### *3.1. Assembly Description*

The assembly consists of welded shapes made from ASTM A36 plates. The column section is H300 × 10 × 16 × 300 mm (length = 3000 mm), and the beam section is H250 × 6 × 10 × 150 mm (clear length = 2350 mm). According to the proposed design procedure, the diameter of the selected bolts is M20 (5/8″), and the bolt pretension applied is 85 kN each, as recommended by AISC 360 [30]. The typical dimensions of the connections, as shown in Figure 1, are S = 60 mm and S1 = 100 mm for the flange bolt pattern. The size and length of the structural members were preliminary selected for a building with steel moment frames located in Santiago, Chile, with three-bay and three-story levels, designed according to seismic loads established in Chilean Code.

The two different locations for the connection (L1 = 375 mm and L1 = 500 mm) reflect the change in the required design load, the two plate thicknesses (e = 8 mm and e = 10 mm) represent both rigid and weakened approaches, and the three different bolt lines affect the energy dissipation (n = 3, 4, and 5 lines). A model M0 consists of a welded beam-to-column connection in order to obtain base results for the maximum moment and energy dissipation; two additional models with L1 = 250 mm and n = 3 are used to analyze the effect of connections as close as possible to the column. Table 1 shows a summary of all analyzed models.

Discretization of the elements was performed, using finer meshing in areas where stress concentration is expected. The boundary conditions simulated the effect of displacement constraints at the column ends. The iteration method used for the nonlinearities was the incremental Newton–Raphson method [31]. In addition, the Augmented Lagrangian method was used to achieve numerical convergence in the contact zone, in accordance with the investigations performed by [32]. Welds were not included in the model because elastic behavior is expected from the design by capacity in the welds. The diameter of the holes used is standard, according to the requirements given in AISC 360 [30].

**Table 1.** Summary of the models studied.

| Model | Distance L1 (mm) | Plate Thickness "e" (mm) | Bolt Lines "n" in Flange Splice |
|---|---|---|---|
| M1 | 375 | 8 | 3 |
| M2 | 375 | 8 | 4 |
| M3 | 375 | 8 | 5 |
| M4 | 375 | 10 | 3 |
| M5 | 375 | 10 | 4 |
| M6 | 375 | 10 | 5 |
| M7 | 500 | 8 | 3 |
| M8 | 500 | 8 | 4 |
| M9 | 500 | 8 | 5 |
| M10 | 500 | 10 | 3 |
| M11 | 500 | 10 | 4 |
| M12 | 500 | 10 | 5 |
| MA | 250 | 8 | 3 |
| MB | 250 | 10 | 3 |
| M0 | - | - | - |

### *3.2. Material Constitutive Law*

A nonlinear, bilinear, kinematic constitutive law and von Mises yield criterion were used. The materials were considered from coupon tests performed according to studies conducted by Nuñez et al. [33] and Herrera et al. [34]. The values are shown in Table 2.

**Table 2.** Constitutive law of materials.

| Material | Fy (MPa) | εy (mm/mm) | Fu (MPa) | εu (mm/mm) |
|---|---|---|---|---|
| ASTM A36 | 294.3 | 0.00146608 | 568.5 | 0.243246 |
| ASTM A-325 | 786 | 0.00393 | 923.897 | 0.16 |

### *3.3. Loading and Boundary Conditions*

The numerical model is representative of real experimental conditions. In this sense, a pinned restriction was applied to the base connection of the column. The end of the beam was deemed to be a simple support with displacement allowed in the vertical direction. Bolt pretension (70% of bolt tension strength) was applied according to the value established in AISC 360 [30]. Also, according to AISC 341 [23], the load was applied to the tip of the link beam through horizontal displacements (Table 3), and lateral supports to the beam were assigned to satisfy the stability criteria. The boundary conditions are shown in Figure 5.

**Table 3.** Load protocol used in the numerical model [23].

| No. | Number of Cycles | Drift Angle (θ) [rad] |
|---|---|---|
| 1 | 6 | 0.00375 |
| 2 | 6 | 0.00500 |
| 3 | 6 | 0.00750 |
| 4 | 4 | 0.0100 |
| 5 | 2 | 0.0150 |

**Table 3.** *Cont.*

| No. | Number of Cycles | Drift Angle (θ) [rad] |
|---|---|---|
| 6 | 2 | 0.0200 |
| 7 | 2 | 0.0300 |
| 8 | 2 | 0.0400 |
| 9 | 1 | 0.0500 |

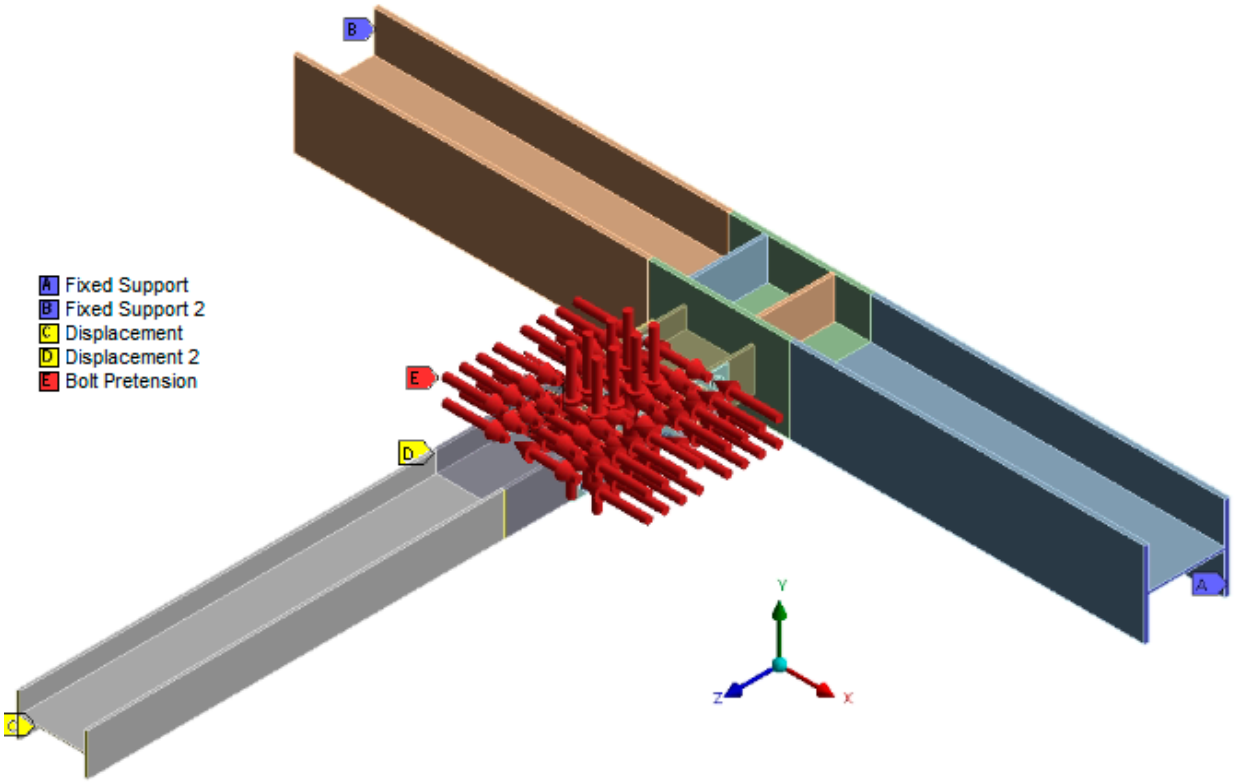



**Figure 5.** Numerical model with boundary conditions.

### *3.4. Elements, Mesh, and Contacts*

The elements and components of the connections in the numerical models were modeled explicitly using the SOLID 186 element. This element is defined by 20 nodes and three degrees of freedom per node in the three principal directions (X, Y, Z). Additionally, this element has a higher capacity to reproduce plasticity, hyperelasticity, creep, stress stiffening, large deflection, and large strain phenomenon. In order to discretize the interest zones, different mesh sizes were considered, ensuring a rational computational cost. Consequently, the solution implemented was to apply a fine mesh in zones with great stresses and coarser mesh in the other regions, as shown in Figure 6.

The contacts used for welded parts are of the "bonded" type, which is equivalent to a fully restrained condition; a "frictional" contact was used to simulate the possible displacement between the components in tight contact, and "frictionless" contacts were used between the bolt shank and the inner face of the holes for the bolts. The friction coefficient varies depending on the surface as-built condition and hole clearance [30]; also, the bolt tightening method could affect the actual applied pretension [18]. However, these parameters are intended to prevent slip at the service load level [35,36], and the static or monotonic response is different than that under cyclic loads. The FEA models only allows the definition of a single mean slip coefficient, in this case, $\mu = 0.2$, to account for a clean mill scale. Table 4 show the type of contacts used in the FEA models.

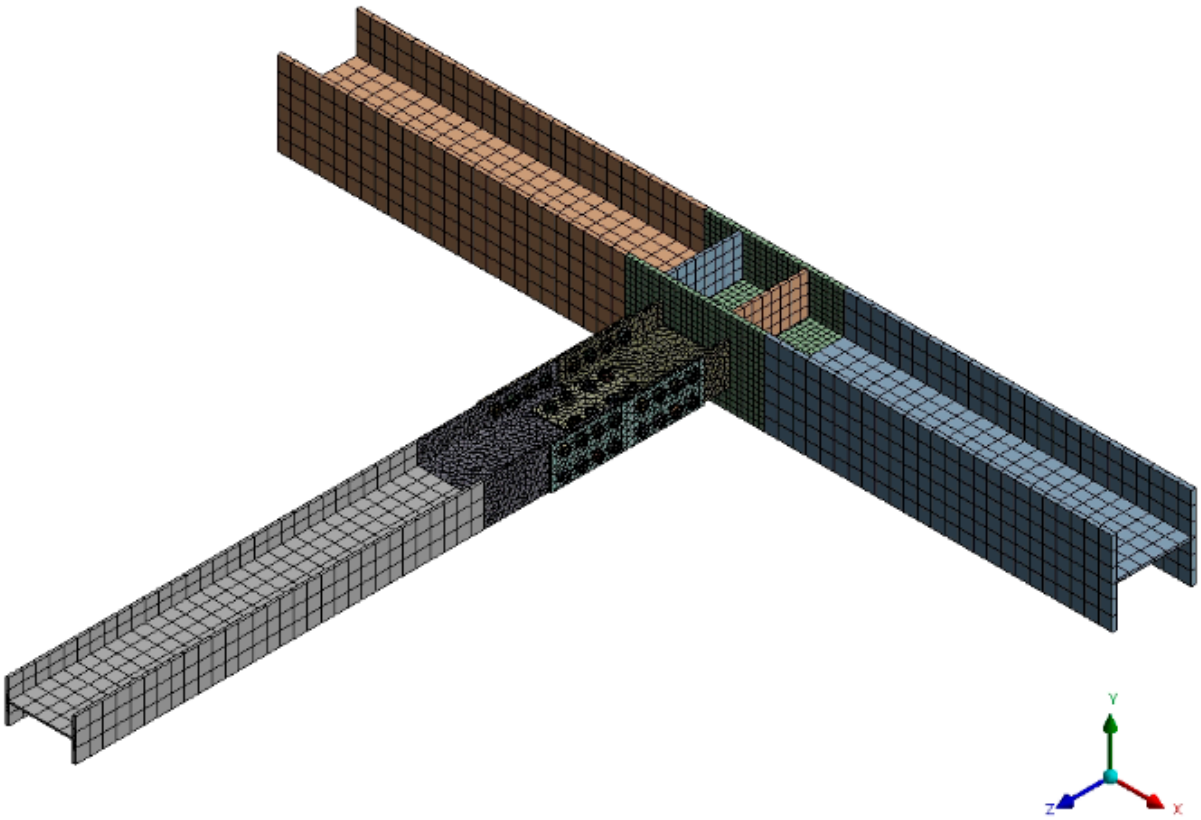



**Figure 6.** Contacts and mesh in numerical models.

**Table 4.** Type of contacts by element in the numerical model.

| No. | Region Interaction | Type of Contact |
|---|---|---|
| 1 | Splice plates–beam | Frictional μ = 0.2 |
| 2 | Bolt shank–plates | Frictionless |
| 3 | Bolt shank–beam | Frictionless |
| 4 | Bolt shank–bolt head | Bonded |
| 5 | Bolt head–splice plates | Frictional μ = 0.2 |
| 6 | Bolt shank–nut | Bonded |
| 7 | Nut–splice plates | Frictional μ = 0.2 |
| 8 | Beam stub–column | Bonded |
| 9 | Column–stiffeners | Bonded |

## 4. Results

### *4.1. Previous Calibration of the Numerical Model*

In order to ensure a representative numerical model, previous calibration of the numerical model was performed based on the experimental research conducted by Oh et al. [22]. Figure 7 shows the mesh, and Figure 8 shows the equivalent stress at the end of the 5% rad cycle. An H600 × 200 × 11 × 7 beam with a length of L = 3500 mm, H400 × 400 × 13 × 21 column, and L1 = 900 mm was used as an assembly in a beam–column joint. The high-strength bolts were of the ASTM A490 type with a pretension of 179 kN and a friction coefficient of 0.2.

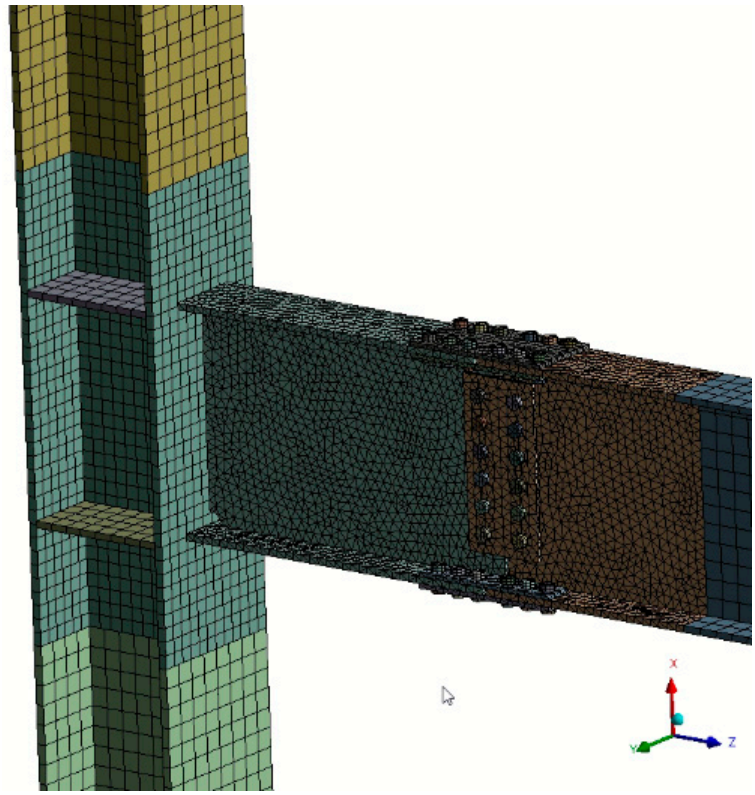


**Figure 7.** Mesh of the calibration numerical model.

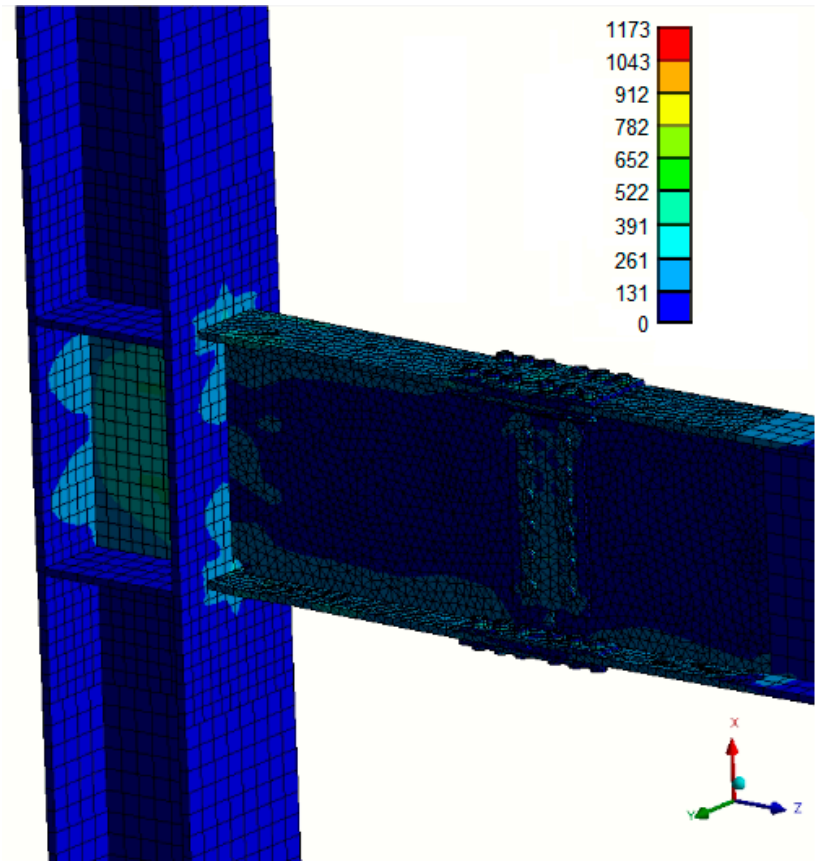



**Figure 8.** Equivalent (von-Mises) stress in the calibration numerical model (MPa).

The calibration hysteresis curve was compared with three specimens tested by Oh et al. [22], obtaining an acceptable adjustment between the numerical model and experimental specimens. Figure 9 shows the results of the numerical model for specimen CT-B performed by Karami et al. [26], the test by Oh et al., and the present study as a comparison to validate the proposed numerical models.

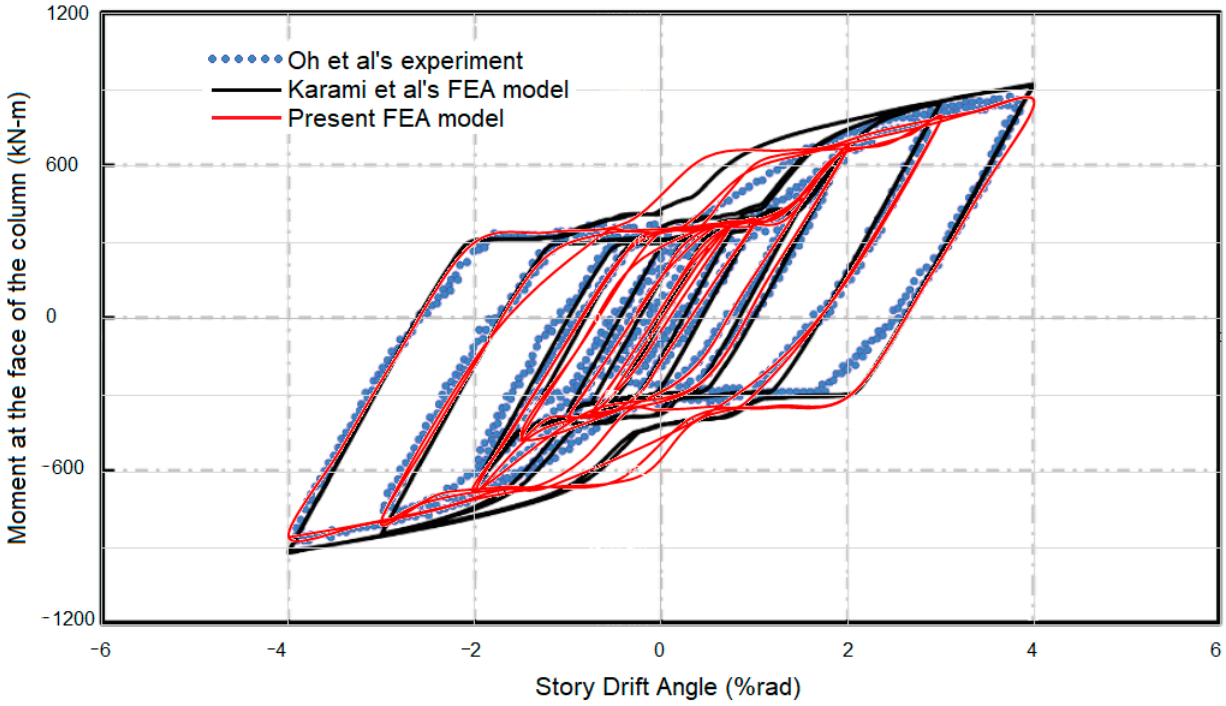



**Figure 9.** Calibration of the numerical model; adapted from Karami et al. [26].

### *4.2. Results of Numerical Models*

In the following text, the hysteretic behavior is reported through a normalized moment–rotation curve. The normalized tangent and secant stiffness are analyzed with the purpose of analyzing the loss of stiffness in the hysteric behavior of the connection. On the other hand, the performance by type of configuration can be analyzed from the dissipated energy, which is an area closed by a loop.

#### 4.2.1. Hysteretic Curve

The summary of normalized moment–rotation for each model is shown in Figures 10–13; all figures include a curve for a beam with a welded connection (base model M0), for comparative purposes. These curves show stable behavior without any significant losses in strength and stiffness. In all cases, the number of bolts does not affect the ultimate strength of the connection. The plate thickness has little effect on the connection strength (but is not proportional to the thickness increase). However, the effect of the number of bolts plateaus at marked different load levels. A summary of the maximum moment at the face of the column is shown in Table 5.

**Table 5.** Summary of maximum normalized moment M/Mp at the column face.

| | | at 0.04 Rad | | at 0.05 Rad | |
|---|---|---|---|---|---|
| **Position** | **Bolts** | **PL8** | **PL10** | **PL8** | **PL10** |
| L1 = 375 mm | n = 3 | 0.98 | 1.07 | 1.07 | 1.15 |
| | n = 4 | 1.00 | 1.09 | 1.08 | 1.16 |
| | n = 5 | 1.01 | 1.11 | 1.09 | 1.19 |

**Table 5.** *Cont.*

| | | at 0.04 Rad | | at 0.05 Rad | |
|---|---|---|---|---|---|
| **Position** | **Bolts** | **PL8** | **PL10** | **PL8** | **PL10** |
| L1 = 500 mm | n = 3 | 1.07 | 1.11 | 1.13 | 1.17 |
| | n = 4 | 1.07 | 1.12 | 1.14 | 1.18 |
| | n = 5 | 1.07 | 1.19 | 1.18 | 1.22 |
| Welded | None | 1.21 | | 1.22 | |

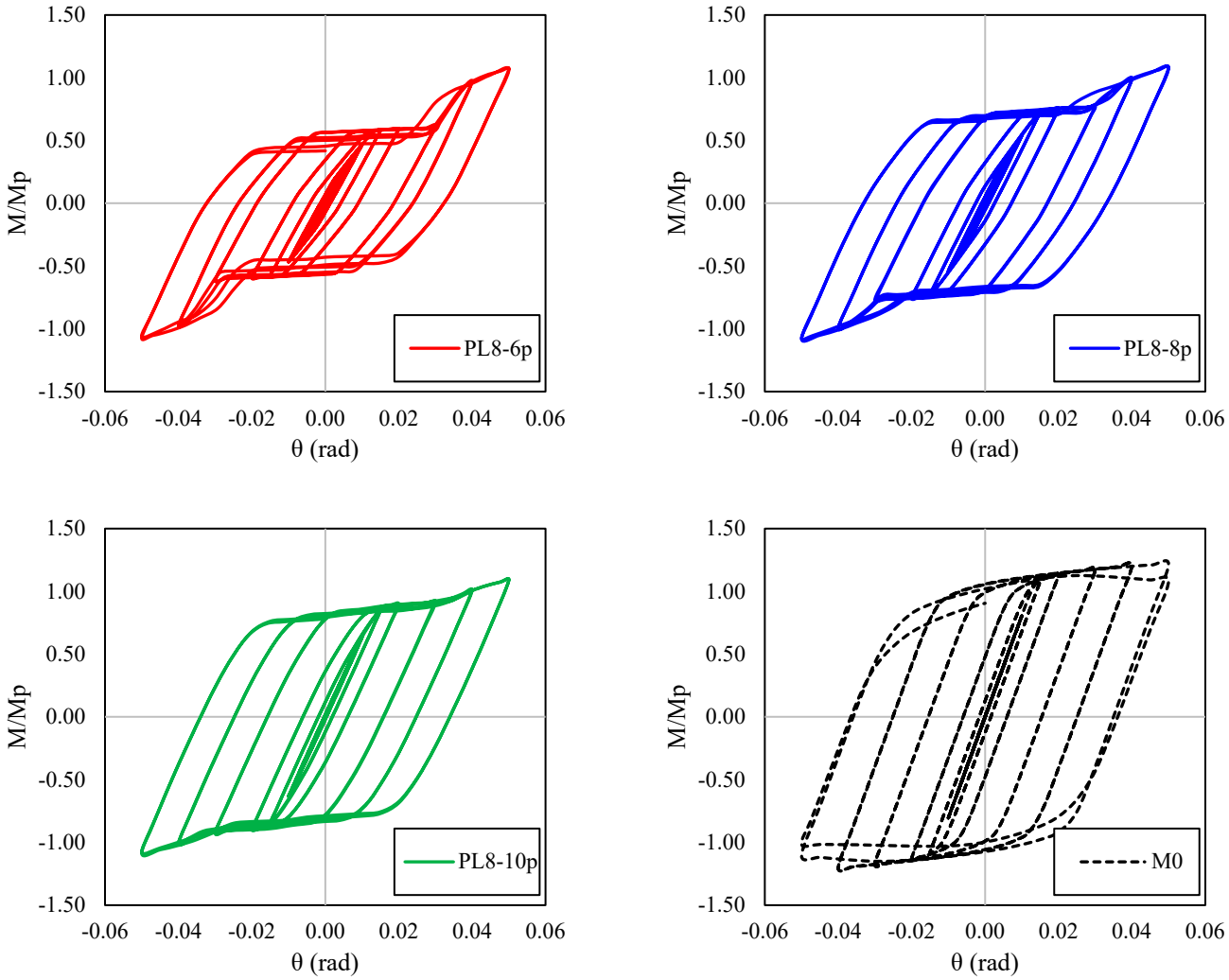



**Figure 10.** Summary of hysteretic curves for models M1 to M3 (L1 = 375 mm and 8 mm plates).

In all cases, the maximum moment at the column face is higher than 1.0 Mp, except for in model M1, which was designed as the weakest connection. For model M12, designed as the strongest case, the hysteretic curve shows that it behaves similarly to the base model M0 with a connection strength of 1.22 Mp.

The connection's ultimate strength depends directly on the selected plate thickness, shown in Figure 14 at the end of the 5% cycle. After the 1% cycle, the relative slip between connection components determines a horizontal segment for every curve, and its magnitude depends on the bolt quantity. Therefore, models with the same bolt quantity (i.e., M1 and M4 or M7 and 10, for example) have similar curves, differing only after the 3% cycle as they have different plate thicknesses. For these "weakened" connections, these two effects can clearly work independently from each other.

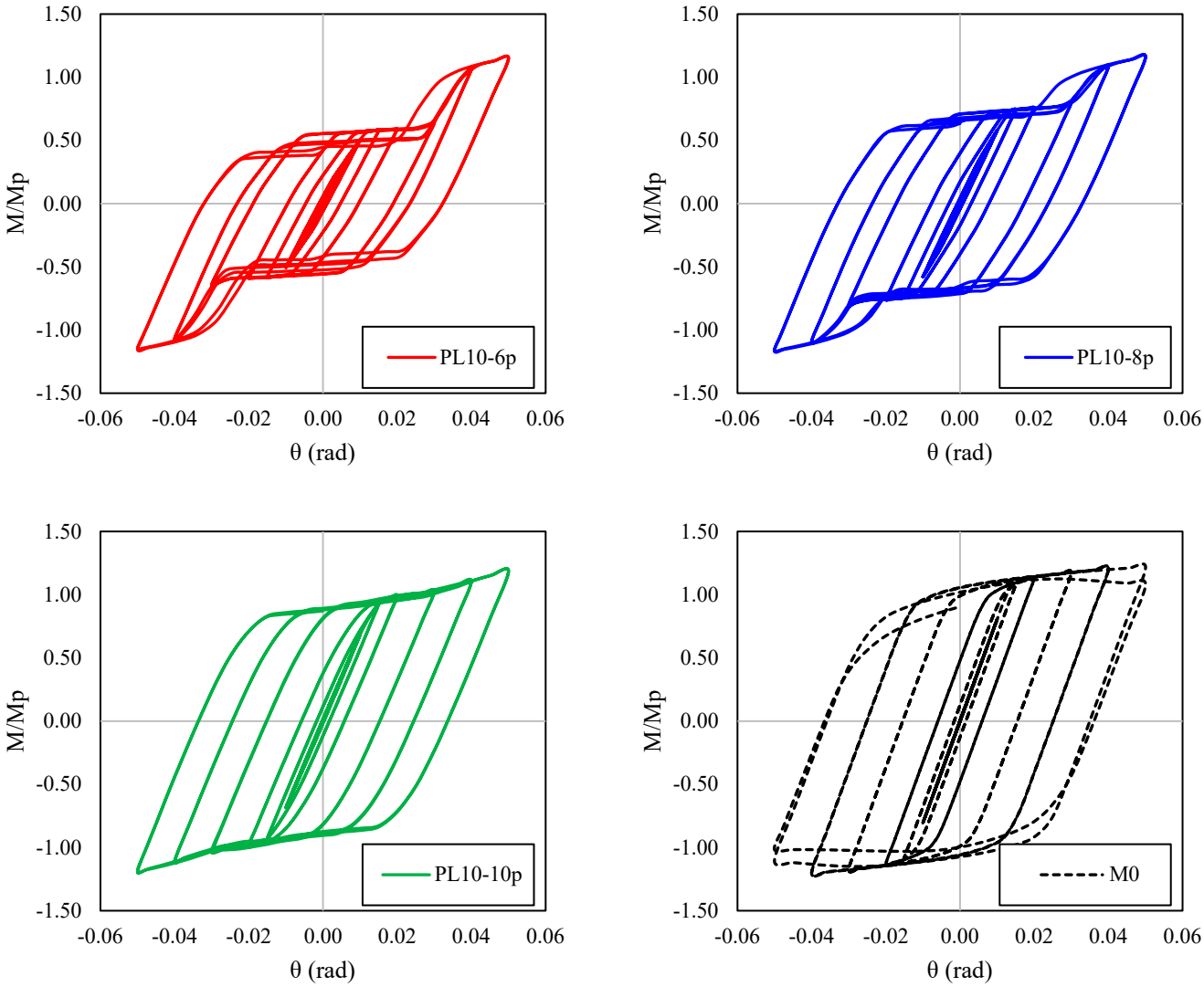



**Figure 11.** Summary of hysteretic curves for models M4 to M6 (L1 = 375 mm and 10 mm plates).

However, for models M6 and M12 (with 10 mm plates and 10 bolts), a synergy effect occurs between both mechanisms, and the horizontal part of the curve for 10 mm plates is located higher than for 8 mm plates. Also, the curve for model M12 (located further from the column) almost matches the curve for the base model M0.

#### 4.2.2. Plastic Strain

Figure 15 shows the plastic deformation of the base model (M0) at the end of the 5% drift cycle. The beam flange local buckling began at the end of the 4% drift as result of a high stress concentration. However, the local buckling was not reported in the models with bolts and cover plates. The plastic strain was concentrated at the splice plates, and in some cases, there was evidence of bearing around the bolt holes at the beam flange. Table 6 shows a qualitative description of the location of the plastic strain concentration.

**Table 6.** Location of the plastic strain concentration at 5% drift.

| Model | Concentration of Plastic Strain | Damage in Stub? |
|---|---|---|
| M1 | Plate ($\varepsilon$pmax = 0.08) | Not reported |
| M2 | Plate ($\varepsilon$pmax = 0.08) | Low |

**Table 6.** *Cont.*

| Model | Concentration of Plastic Strain | Damage in Stub? |
|---|---|---|
| M3 | Plate (εpmax = 0.12) | Low |
| M4 | Plate/Stub (εpmax = 0.09) | Medium |
| M5 | Stub (εpmax = 0.10) | High |
| M6 | Stub (εpmax = 0.10) | High |
| M7 | Plate (εpmax = 0.08) | Not reported |
| M8 | Plate/Stub (εpmax = 0.08) | Medium |
| M9 | Plate (εpmax = 0.09) | Medium |
| M10 | Stub (εpmax = 0.09) | Medium |
| M11 | Stub (εpmax = 0.10) | Stub |
| M12 | Stub (εpmax = 0.06) | Stub |

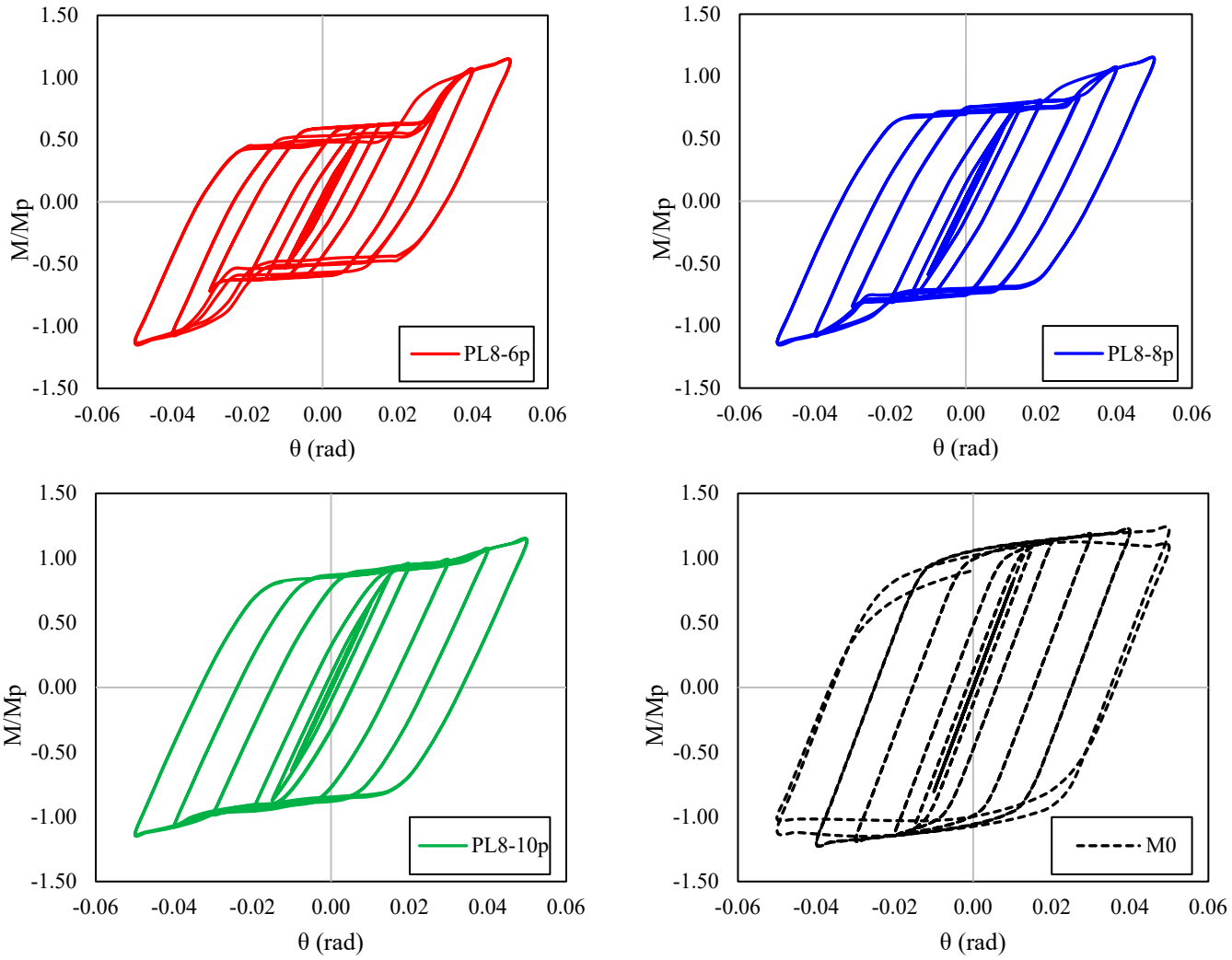



**Figure 12.** Summary of hysteretic curves for models M7 to M9 (L1 = 500 mm and 8 mm plates).

Figure 16 shows the plastic strain at the end of the 5% cycle for the models with L1 = 375 mm. Models M1, M2, and M3 with 8 mm plates present moderate damage for the cases with fewer bolts, while model M3 shows no damage at all, meaning that most of the energy is dissipated through friction. Figure 17 shows that models M4, M5, and M6 with

10 mm plates are stiffer, and some damage occurs at the beam stub flanges instead of at the splice plates. Plastic strain in the stub was reached for models M4 and M6, because the cover plates are more rigid and closer to the column. This effect was not reported in models M1, M2, and M3.

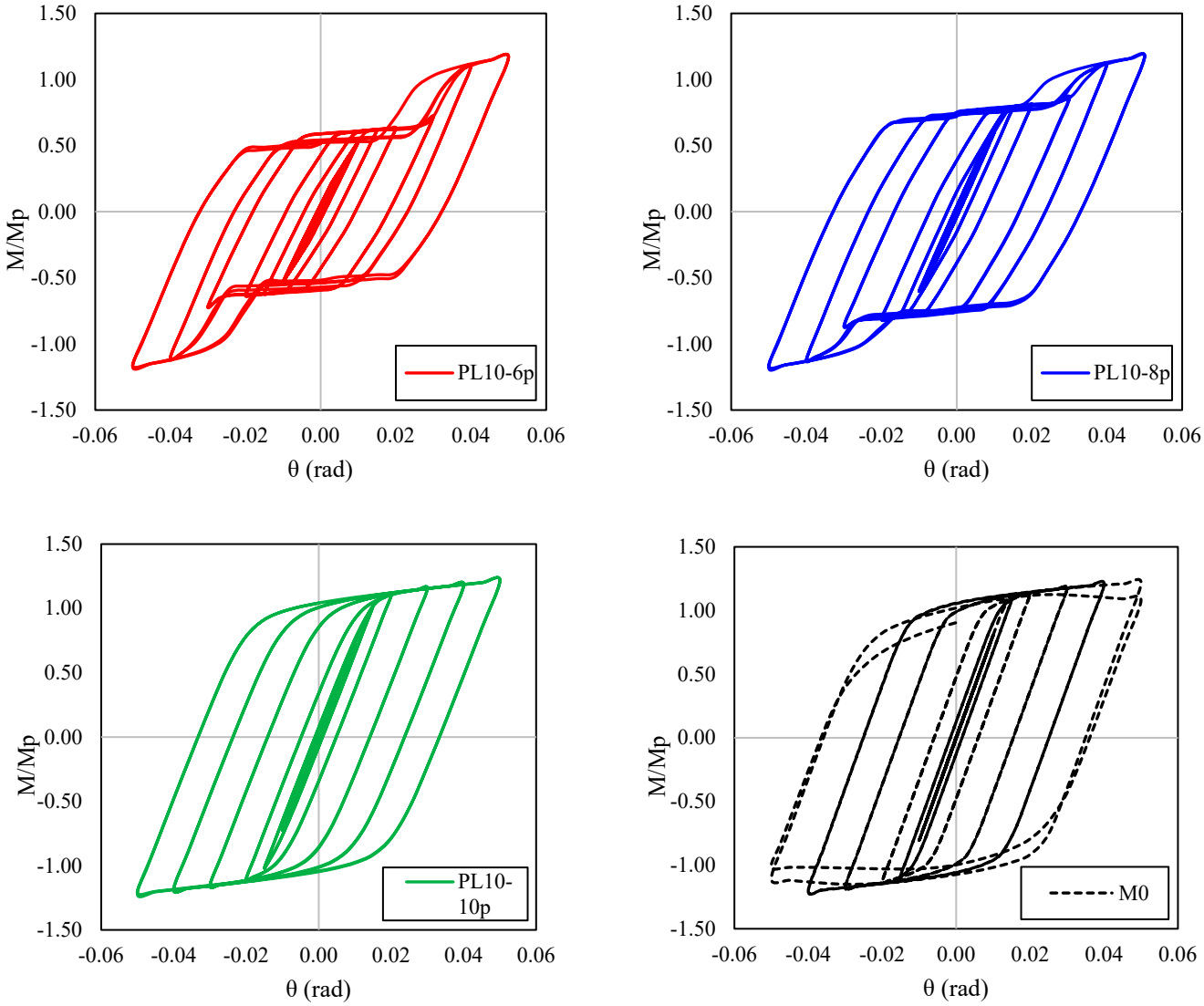



**Figure 13.** Summary of hysteretic curves for models M10 to M12 (L1 = 500 mm and 10 mm plates).

Figure 18 shows the plastic strain at the end of 5% cycle for the models with L1 = 500 mm. Models M7, M8, and M9 with 8 mm plates present moderate damage for the cases with fewer bolts, while model M9 shows less damage, meaning that most of the energy dissipated through friction. Figure 19 shows that models M10, M11, and M12 with 10 mm plates are stiffer, and little damage occurs at the beam stub flanges in the weld's vicinity. However, model M12 presents a high level of damage in the stub. These results are similar to those obtained by Oh et al. [22] for specimens designed with higher strength (specimen CT).

It is observed that when the extension of the connection plate (with more bolts) results in a smaller gap or distance to the column face, damage concentration occurs at the beam stub (models M6 and M12).

#### 4.2.3. Stiffness Curves

According to the AISC specification [30], the nonlinear behavior of the connection manifests, even at low moment–rotation levels, or exists only for a limited moment–rotation

range. The secant stiffness, $Ks = {}^{Ms}/_{\theta s}$, at service loads is taken as an appropriate parameter for the connection, where Ms is the moment at the service loads and θs is the rotation at the service loads. Implicit in the moment–rotation curve is the definition of the connection as being a region of the column and beam, along with the connecting elements. Then, the ratio between the connection rotational stiffness Ks and the beam rotational stiffness (IE/L) is used to classify the connection as fully rigid (FR), partially rigid (PR), or flexible (F). Figure 14 shows an overview of the tangent and secant stiffness from the backbone curves of the assemblies. The connection relative rotation due to bolt slip does not allow for the direct determination of the tangent stiffness, although a tangent stiffness tendency is shown after the 4% cycle when the bolt clearance limits further slippage.

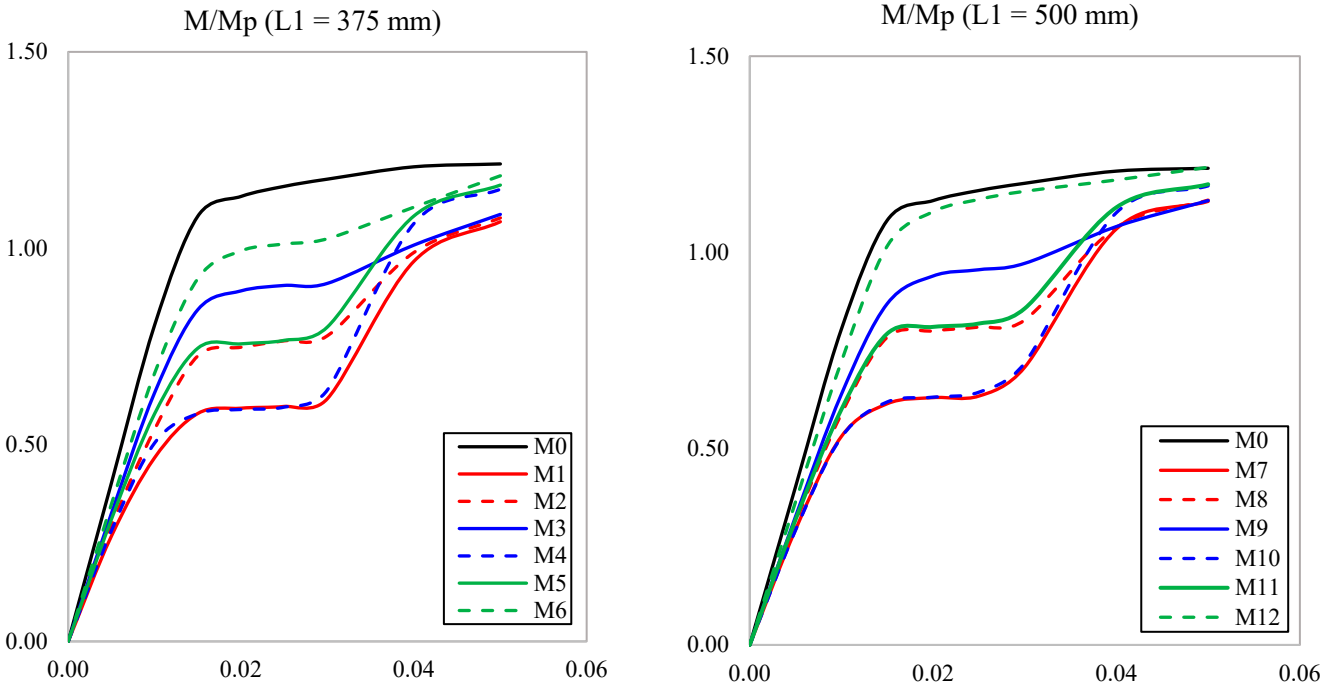



**Figure 14.** Summary of backbone curves, M/Mp, at the column face.

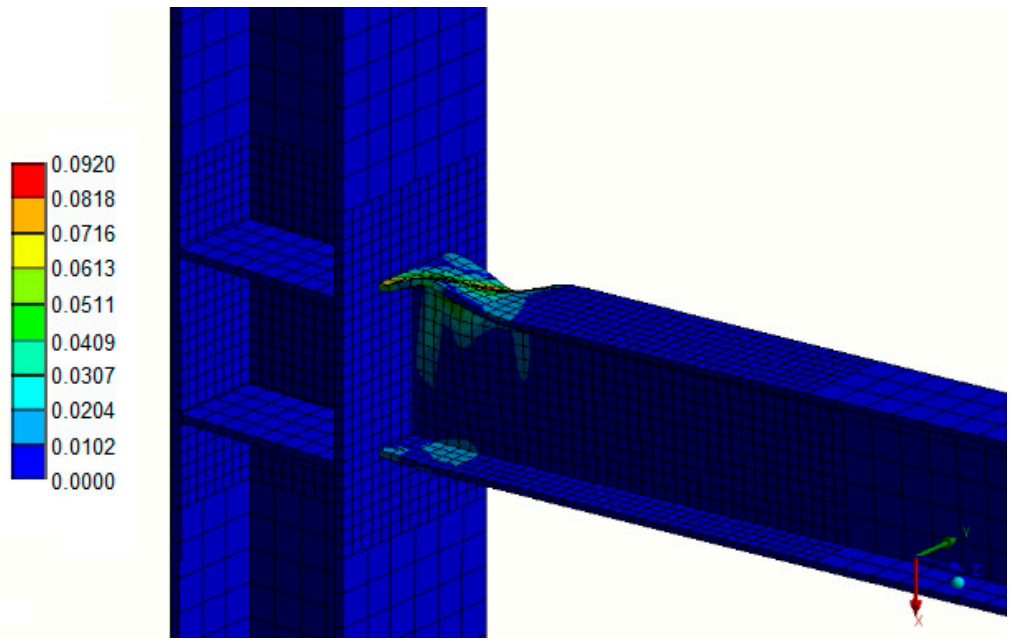



**Figure 15.** Plastic strain for the base model M0 (mm/mm).

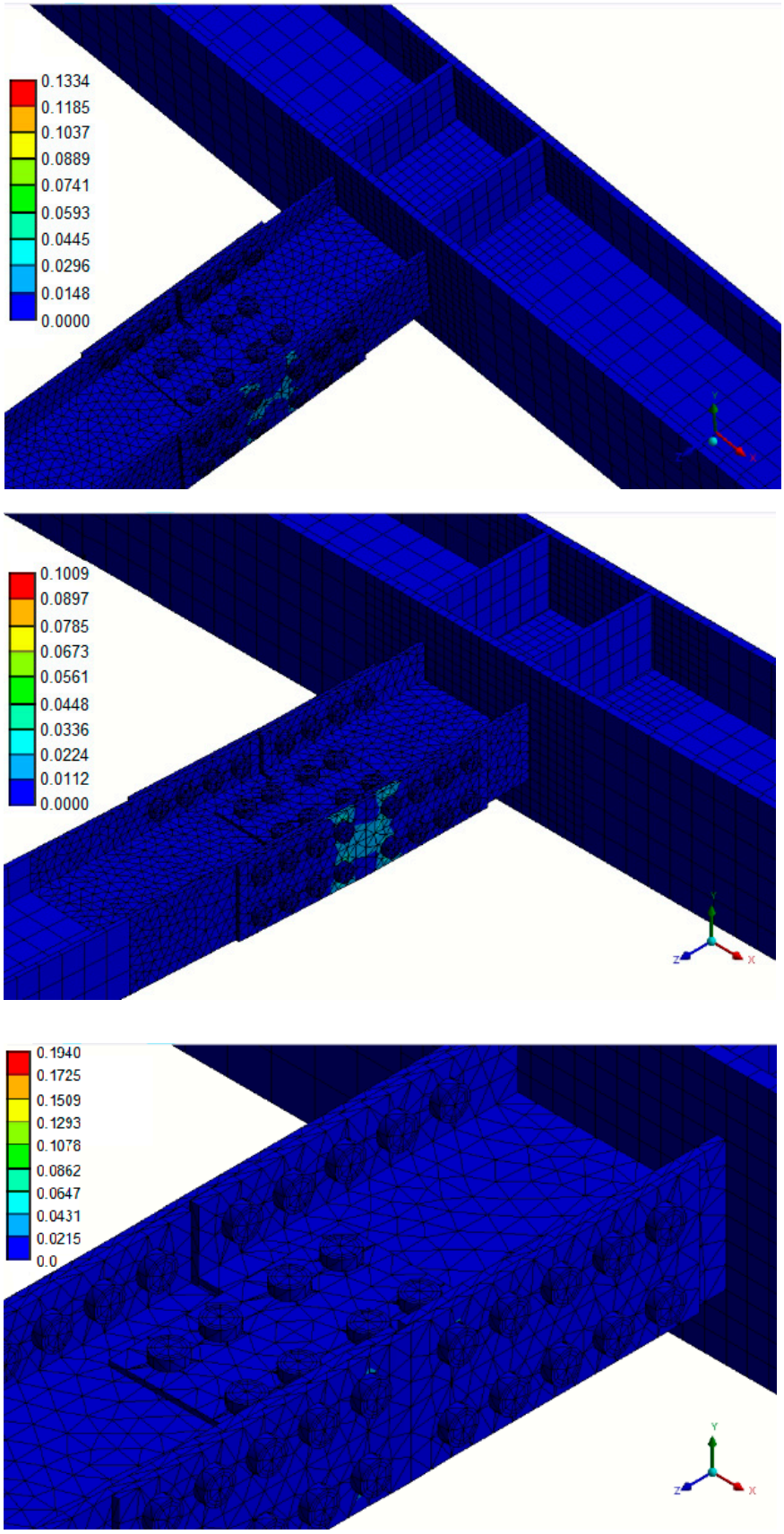



**Figure 16.** Plastic strain for models M1, M2, and M3 (from top to bottom) (mm/mm).

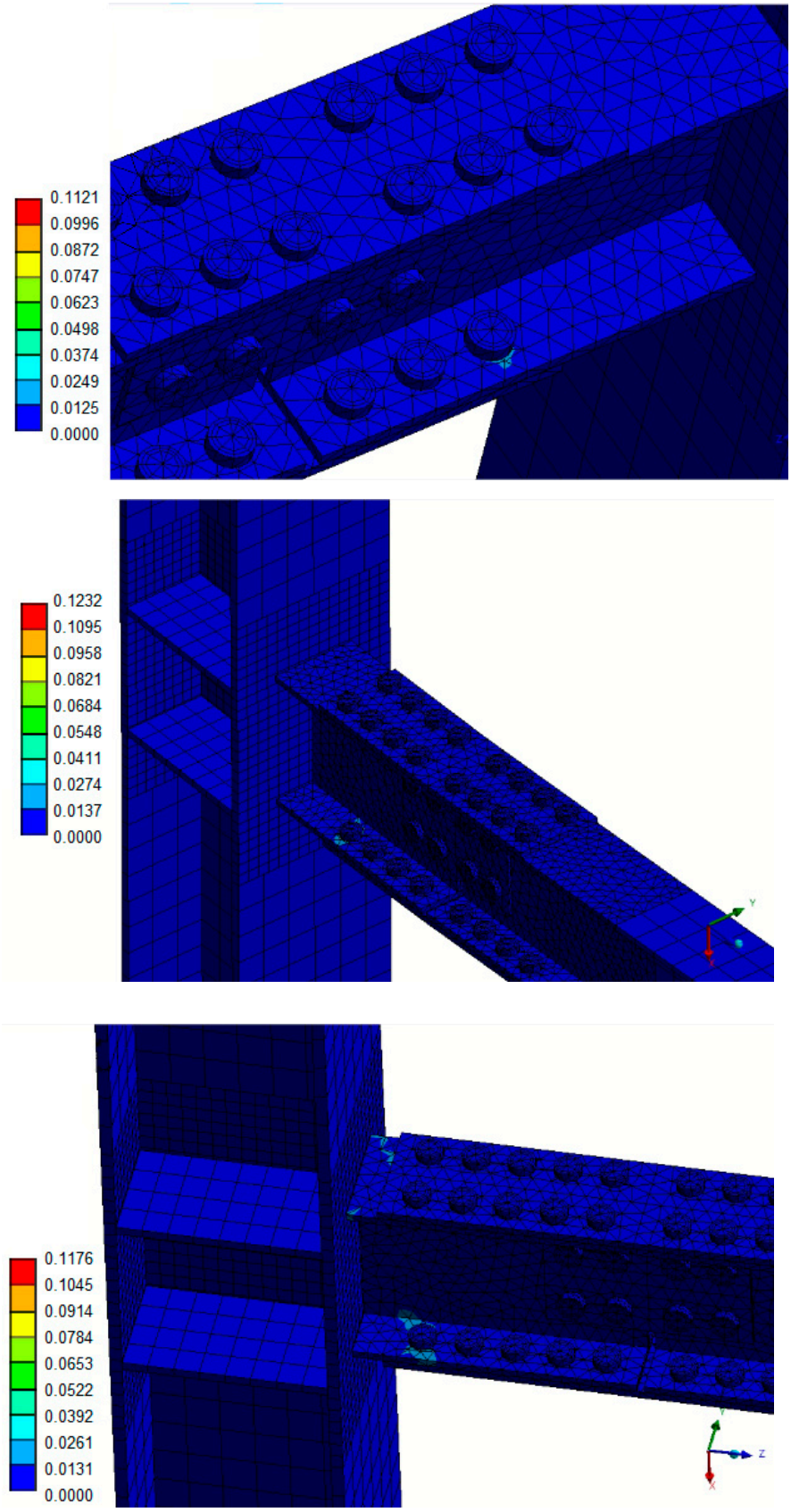



**Figure 17.** Plastic strain for models M4, M5, and M6 (from top to bottom).

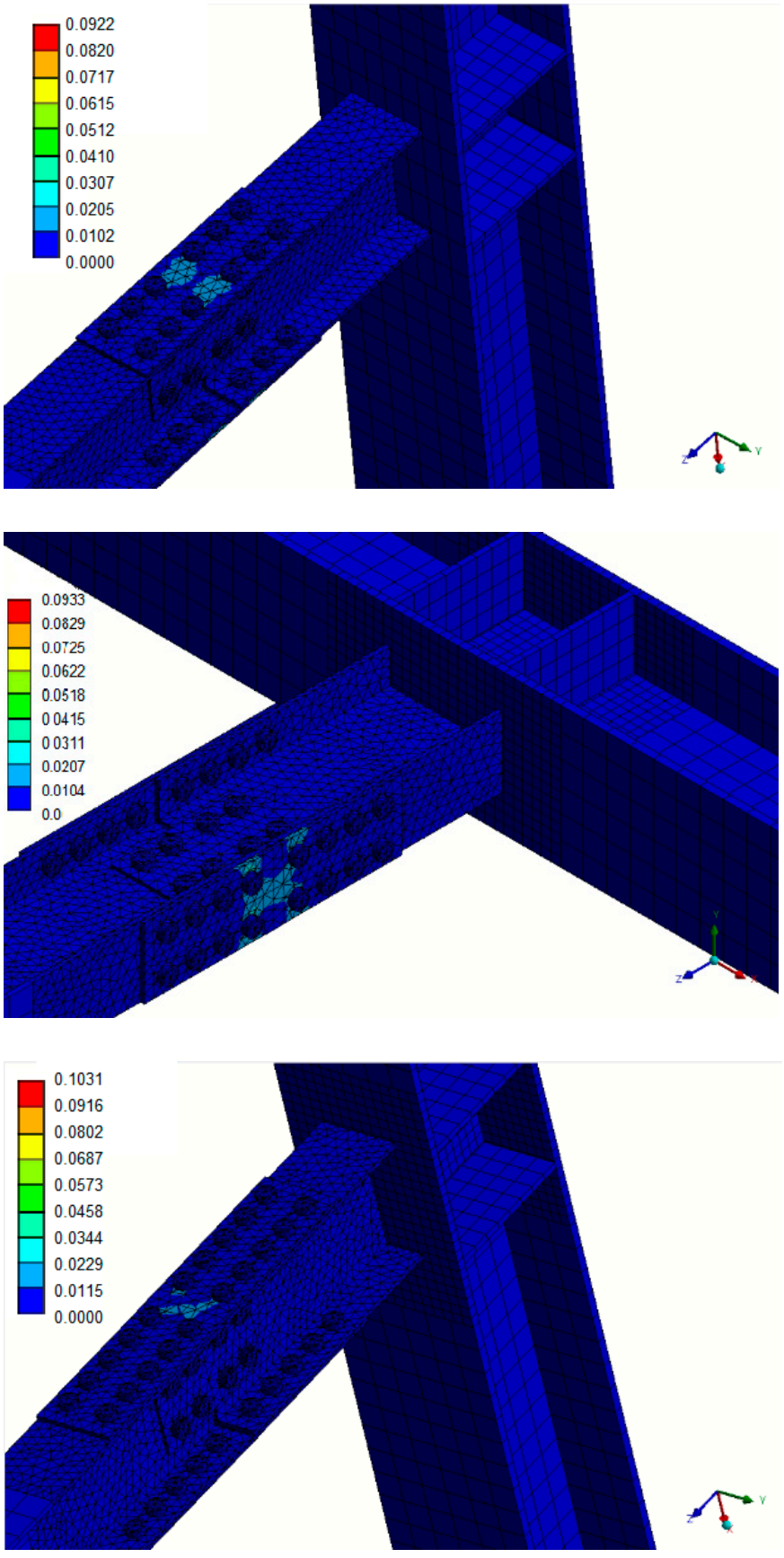



**Figure 18.** Plastic strain for models M7, M8, and M9 (from top to bottom) (mm/mm).

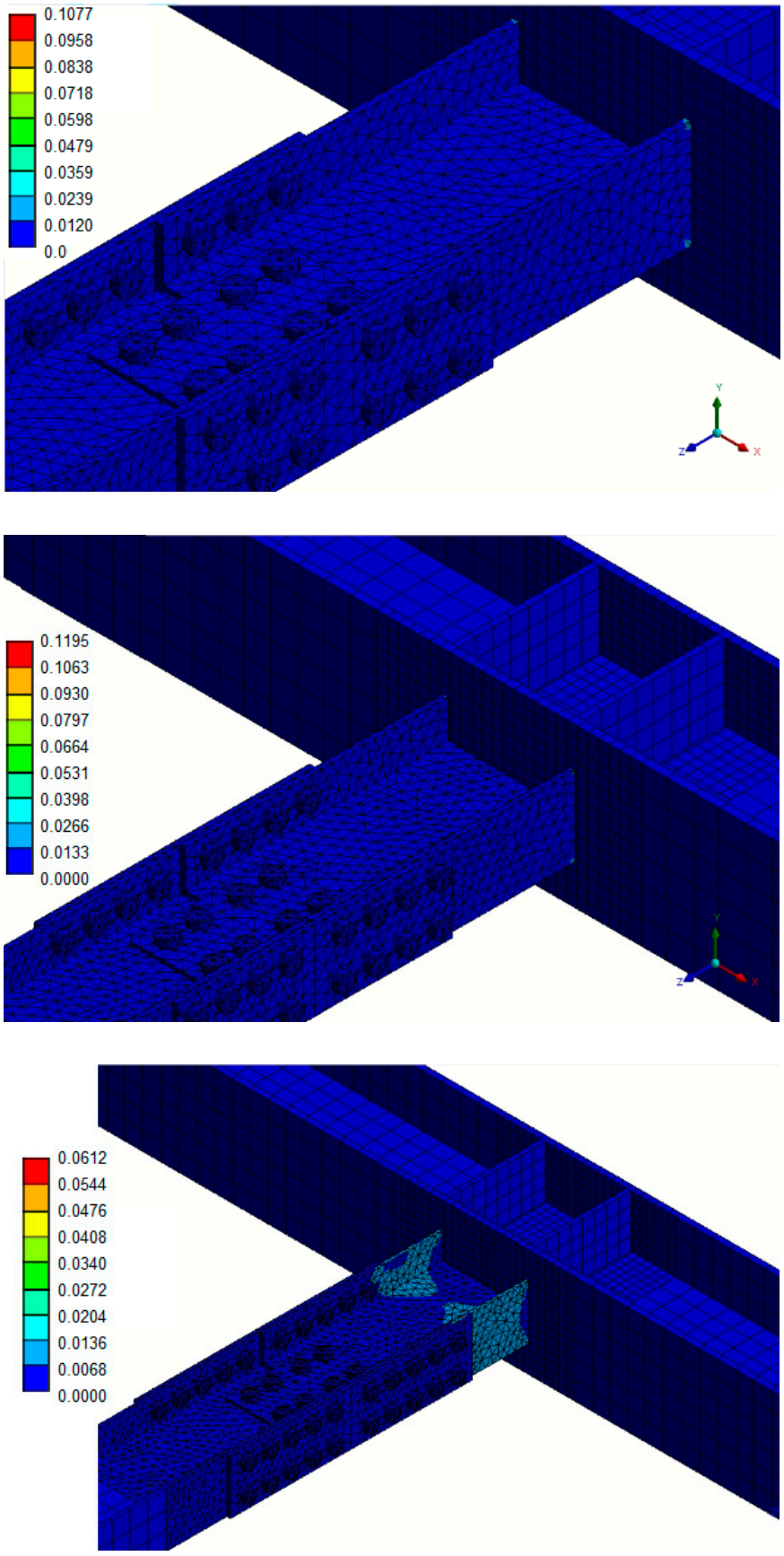



**Figure 19.** Plastic strain for models M10, M11, and M12 (from top to bottom) (mm/mm).

Astaneh-Asl [16] suggests that, for column-tree systems where the length of the beam stub is less than 0.15 of the span length L, the rotational stiffness of the bolted splice Ksp should be used instead. Figure 20 shows the backbone curves for the bolted splice for moment and rotation at the splice location, where the secant stiffness Ksp can be calculated. However, the "service load" level is not clearly defined for the seismic demand; this study assumes that Ms = Sx × Fy, which is the moment that causes the initial yielding of the beam flange; in this way, the service load aims to avoid damage at the beam stub.

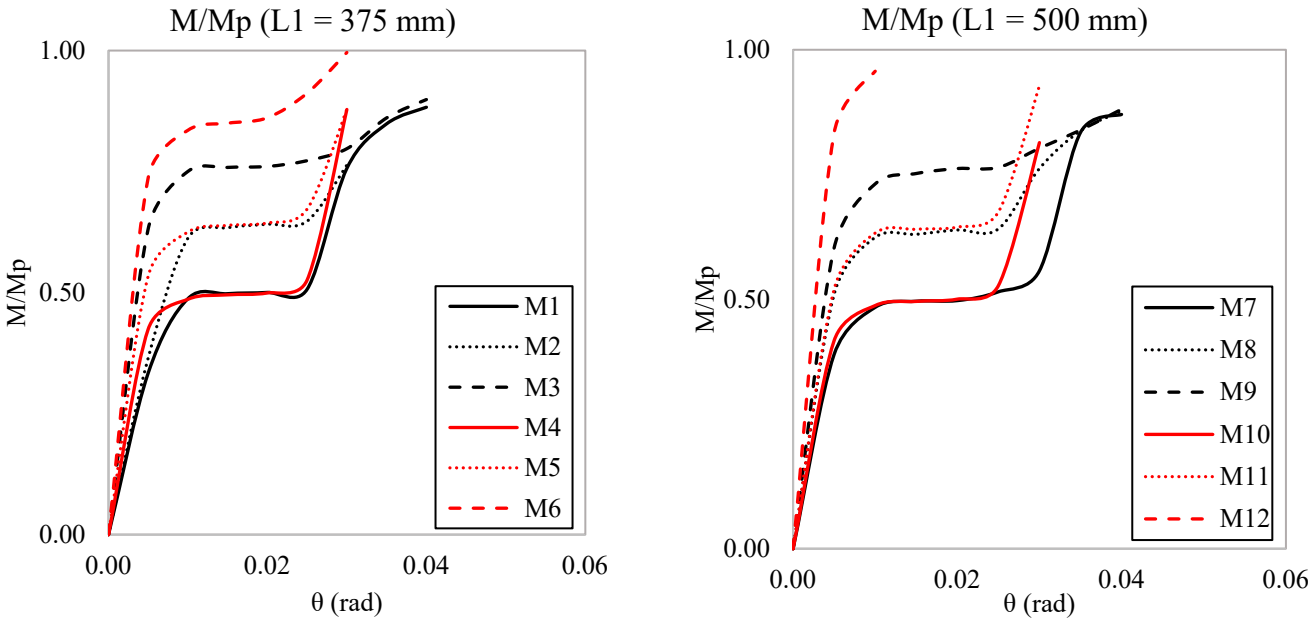



**Figure 20.** Summary of backbone curves for bolted connections.

Table 7 shows the parameters used for the calculation of the rotational stiffness of the models included in the study.

**Table 7.** Parameters of the H250 × 6 × 150 × 10 beam.

| | | |
|---|---|---|
| Beam Mp | 109.4 | kN-m |
| Beam My | 98.2 | kN-m |
| Beam Ixx | 437.5 | cm4 |
| Beam length | 4.7 | m |
| Steel E | 200,000 | Mpa |
| EI/L | 2159 | kN-m/rad |

Table 8 shows the rotational stiffness parameters for the analyzed models. Those with six bolts per flange are the most flexible with m-s < 2. They are classified as simple connections due to the early relative slippage of the components. The rest of the models are classified as PR and have a tendency to increase their stiffness when using thicker plates (i.e., 12 mm) or more bolts (i.e., 12 per flange).

**Table 8.** Stiffness parameters for the H250 × 6 × 150 × 10 beam.

| Model | Mreq | Mplate | Mslip | Ksp-e | Ksp-s | m-e | m-s | Type |
|---|---|---|---|---|---|---|---|---|
| M1 | 92 | 77.1 | 31.9 | 11,239 | 2859 | 5.21 | 1.32 | Simple |
| M2 | 92 | 77.1 | 42.5 | 13,800 | 6748 | 6.39 | 3.13 | PR |

**Table 8.** *Cont.*

| Model | Mreq | Mplate | Mslip | Ksp-e | Ksp-s | m-e | m-s | Type |
|---|---|---|---|---|---|---|---|---|
| M3 | 92 | 77.1 | 53.1 | 16,222 | 15,414 | 7.51 | 7.14 | PR |
| M4 | 92 | 97.1 | 31.9 | 12,856 | 2808 | 5.95 | 1.30 | Simple |
| M5 | 92 | 97.1 | 42.5 | 16,143 | 6824 | 7.48 | 3.16 | PR |
| M6 | 92 | 97.1 | 53.1 | 22,631 | 23,028 | 10.48 | 10.67 | PR |
| M7 | 86 | 77.1 | 31.9 | 13,004 | 2918 | 6.02 | 1.35 | Simple |
| M8 | 86 | 77.1 | 42.5 | 15,915 | 11,910 | 7.37 | 5.52 | PR |
| M9 | 86 | 77.1 | 53.1 | 17,638 | 13,417 | 8.17 | 6.21 | PR |
| M10 | 86 | 97.1 | 31.9 | 13,851 | 3247 | 6.42 | 1.50 | Simple |
| M11 | 86 | 97.1 | 42.5 | 17,363 | 13,833 | 8.04 | 6.41 | PR |
| M12 | 86 | 97.1 | 53.1 | 26,858 | 29,514 | 12.44 | 13.67 | PR |

Mreq: required moment strength at the splice location (kN-m); Mplate: moment strength of the splice plates—yielding (kN-m); Mslip: moment strength of the bolt group—slip (kN-m); Ksp-e: bolted splice rotational stiffness at the elastic load level (kN-m/rad); Ksp-s: bolted splice rotational stiffness at the service load level (kN-m/rad); m-s: stiffness parameter for the connection classification (m = Ksp-s/(EI/L).

#### 4.2.4. Energy Dissipation

In Figure 21, the results show that an increment in the quantity of bolts has a notorious positive effect on the cumulative energy dissipation over time. However, an increment in the plate thickness does not have a relevant effect. In Figure 22, the results show that the location of the connection is not relevant for energy dissipation, with a slight increment for L1 = 500 mm.

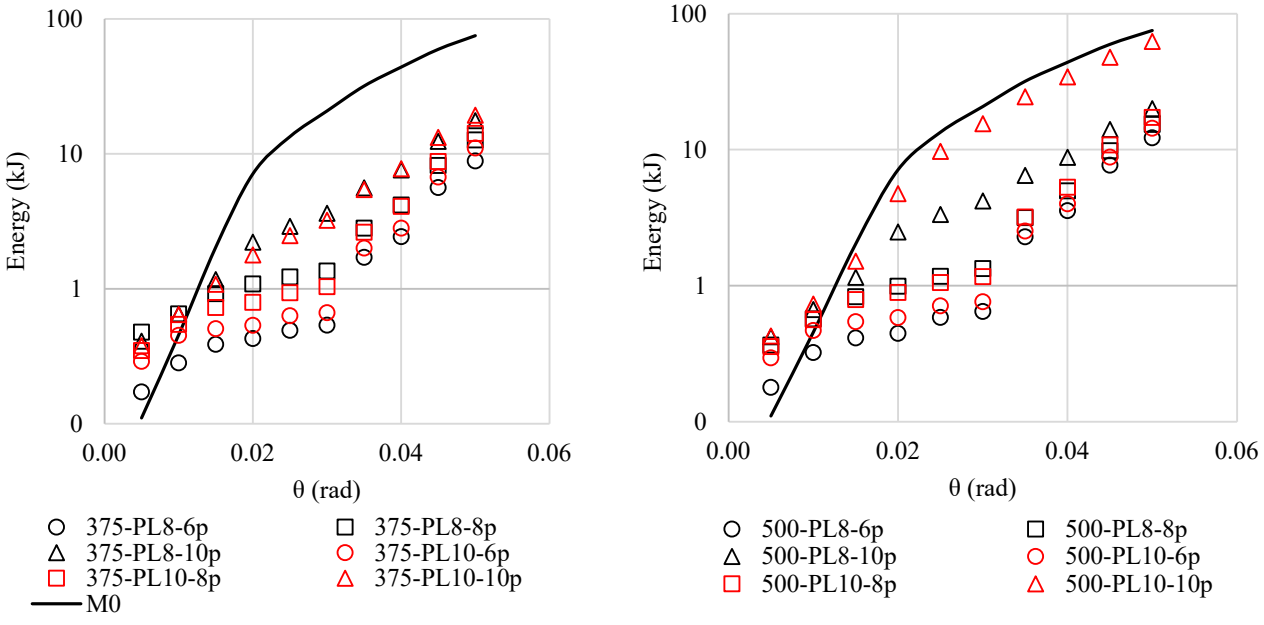



**Figure 21.** Summary of the energy dissipation (kJ) for all models analyzed for models M1@M6 (**left**) and models M7@M12 (**right**). Black line represents the model M0 (welded beam).

#### 4.2.5. Bolted Splice Ductility

The bolted splice ductility m is the ratio between the inelastic rotation (θu–θy) and the elastic limit θy. For the present study, the connection strength was set at a rotation equal to θu = 4% drift. The results are summarized in Table 9. As the connection stiffens (more bolts, thicker plates), its ductility reduces. An increase in the beam stub length causes a slight increase in the connection ductility.

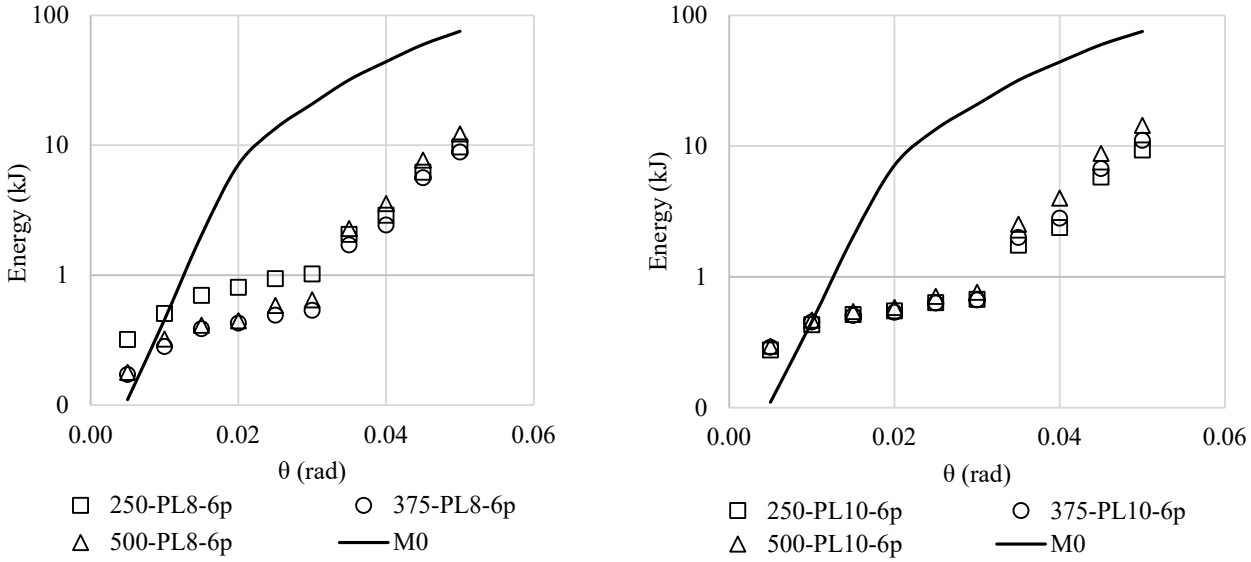



**Figure 22.** Summary of the energy dissipation for different locations of connection (kJ). Models M0, M1, and M7 (**left**) and models M0, M4, and M10 (**right**). Black line represents the model M0 (welded beam).

**Table 9.** Summary of the connection ductility.

| Model | θy | θu | μ |
|---|---|---|---|
| M1 | 0.37% | 3.37% | 8.1 |
| M2 | 0.46% | 3.35% | 6.3 |
| M3 | 0.71% | 3.41% | 3.8 |
| M4 | 0.33% | 3.12% | 8.5 |
| M5 | 0.41% | 3.01% | 6.3 |
| M6 | 0.56% | 2.75% | 3.9 |
| M7 | 0.34% | 3.44% | 9.1 |
| M8 | 0.41% | 3.36% | 7.2 |
| M9 | 0.66% | 3.35% | 4.1 |
| M10 | 0.48% | 3.07% | 5.4 |
| M11 | 0.74% | 2.94% | 3.0 |
| M12 | 0.41% | 0.81% | 1.0 |

Ductility is also related to damage, in this case, in the form of plastic deformation. Model M0 is shown in Figure 15, with evident damage at the flange buckling. Table 10 shows that, for a connection closer to the column face (L1 = 375 mm), the quantity of bolts is the main factor that affects the connection ductility. For the connections located far from the column (L1 = 500 mm), the ductility is affected by both the bolt quantity and the plate thickness.

**Table 10.** Ductility for different bolt quantities and plate thicknesses.

| L1 = 375 mm | e = 8 mm | e = 10 mm | L1 = 500 mm | e = 8 mm | e = 10 mm |
|---|---|---|---|---|---|
| 6 bolts | 8.1 | 8.5 | 6 bolts | 9.1 | 5.4 |
| 8 bolts | 6.3 | 6.3 | 8 bolts | 7.2 | 3.0 |
| 10 bolts | 3.8 | 3.9 | 10 bolts | 4.1 | 1.0 |

## 5. Discussion

A comparison between the different parameters of the connection behavior is developed, as follows.

### *5.1. Location Effect*

As the connection is located away from the column face, the moment required at the bolted splice decreases, and its relative stiffness increases. The overall effect is an increase of 1% to 6% in the tension at the welds and the beam stub flanges, as shown in Table 11. There is no significant increase in the energy dissipation.

**Table 11.** Comparison of the moments at the column face for different splice locations with a 5% drift cycle.

| L = 375 mm | M/Mp | L = 500 mm | M/Mp | M500/M375 |
|---|---|---|---|---|
| M1 | 1.07 | M7 | 1.13 | 106% |
| M2 | 1.08 | M8 | 1.13 | 105% |
| M3 | 1.09 | M9 | 1.13 | 104% |
| M4 | 1.15 | M10 | 1.17 | 102% |
| M5 | 1.16 | M11 | 1.17 | 101% |
| M6 | 1.18 | M12 | 1.22 | 103% |

For practical purposes, this variable can be useful to set a desired connection stiffness.

### *5.2. Plate Thickness Effect*

The main effect of the plate thickness is the connection stiffness. Figure 23 shows that the plate thickness does not have a significant effect on the ultimate connection strength; however, a thinner plate does lower the reaction at the column face, decreasing the plastic strain (damage) at the beam stub flanges.

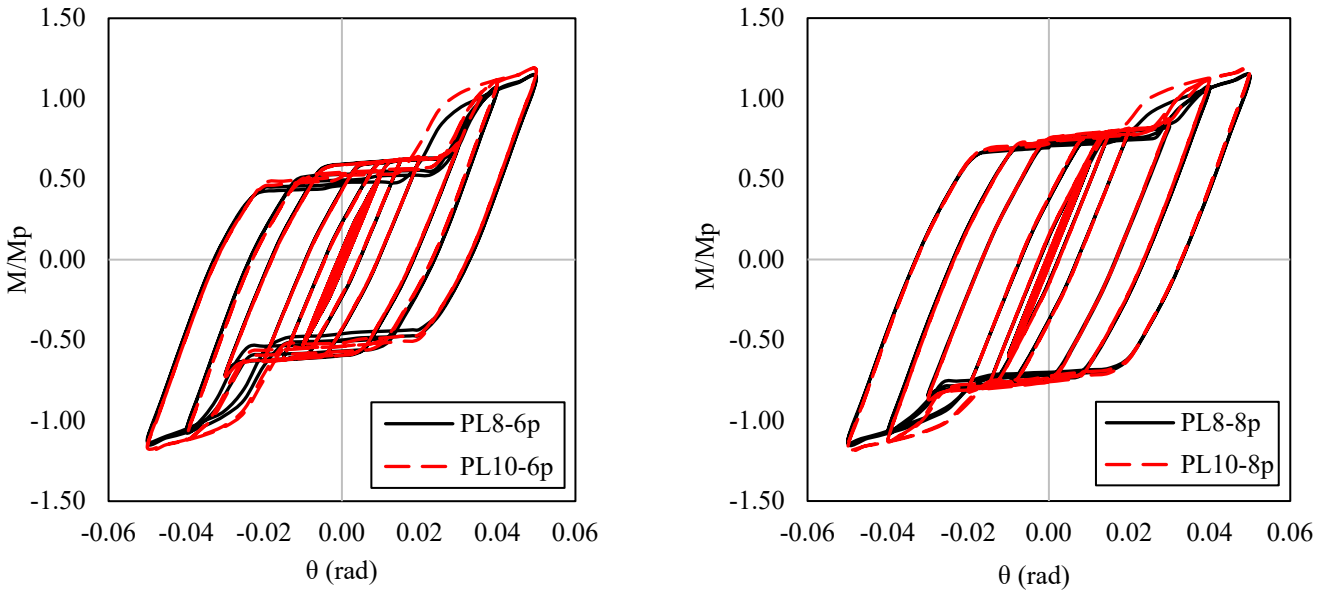



**Figure 23.** Effect of the splice plate thickness on the connection strength for six bolts (**left**) and eight bolts (**right**), for L1 = 500 mm.

The plate thickness plays a secondary role to the bolt quantity and is harder to predict. A thinner plate is more prone to deformation and deflection, increasing the tension at the flange bolts closer to the connection center. The result is a loss in the friction resistance.

### *5.3. Bolt Quantity Effect*

The main effect of the bolt quantity is the energy dissipation (see Figure 21). Given a minimum quantity to provide a bearing shear capacity, the plates slip at low cycle loads preventing the connection from taking advantage of the friction work. A higher number of bolts means more friction and a higher potential for energy dissipation. However, if the slip strength of the bolt group reaches or surpasses the plastic moment of the splice plates, slippage takes place only at the last load cycles.

Therefore, a specific feature effect of the bolt quantity is the staggered shape of the hysteretic curve (see Figure 14), which means that a lower number of bolts reduces the stiffness of the connection after it reaches its slip strength, protecting the beam stub from developing early plastic strain. More studies on this topic may lead to a procedure being found to determine the optimum number of bolts to maximize the energy dissipation of the connection while minimizing the damage to the beam and the column.

## 6. Conclusions

In column-tree moment connections, the bolted splice is usually designed to be stronger than the connected beams and does not affect the seismic performance of the frame. However, if the moment connection is designed as semi-rigid in a selected location away from the column, the connection can develop the ability to effectively reduce the seismic forces and provide a good source of energy dissipation. The goal of this research was to assess the cyclic performance of column-tree moment connections using weakened plates. The newly proposed approach was evaluated in analytical and numerical studies using the finite element model with ANSYS. A total of fourteen nonlinear models were developed, simulating a full-scale test of joints with a built-up H-column to I-beam subjected to the AISC seismic provisions loading protocol. A previous calibration from the experimental test was performed. The main conclusions obtained are described as follows:

(1) The 80% of plastic moment was reached at an interstory drift ratio of 0.04 for all cases analyzed. However, a pinching of the hysteretic curve was obtained for models with a combined failure mechanism (failure in plates and stub) and failure in plates.
(2) The selected location for the bolted splice does not affect the overall performance of the connection. However, models with a length stub of 250 mm (MA, MB, and M6) showed that, when located too close to the column, a collateral effect of over-stiffness induced a stress concentration in the vicinity of the beam-to-column weld.
(3) The weakened connections effectively reduced the plastic strain at the beam-to-column welds and at the beam stub itself. Hence, the connection plates performed well as damage-control fuses that can be replaced easily after a severe seismic event. Also, the thickness plate has a marginal effect on the ultimate strength of the connection, and the bolt quantity does not play a major role in the connection strength.
(4) According to the classification of moment connections established in AISC 360, the column-tree moment connection using weakened plates proposed in this research is classified as partially restrained (PR). Therefore, the seismic design of steel buildings with moment frames using this type of moment connection should consider the elastic stiffness of the connection to verify the drift limits.
(5) Finally, damage after a severe earthquake will mostly develop as plastic deformation of the connection plates, which can be replaced in a cost-effective manner. This change in philosophy regarding the use of replaceable components as fuse components over the use of a beam as a fuse member was demonstrated in the experimental tests carried out by the authors.

**Author Contributions:** Conceptualization, E.N.; methodology, E.N.; software, P.M.; validation, E.N. and P.M.; formal analysis, P.M.; investigation, P.M.; resources, P.M. and E.N.; data curation, E.N.; writing—original draft preparation, P.M.; writing—review and editing, P.M.; visualization, E.N.; supervision, E.N.; project administration, E.N.; funding acquisition, P.M. and E.N. All authors have read and agreed to the published version of the manuscript.

**Funding:** The research reported herein was possible thanks to the funding of Proyectos Ingeniería 2030 (ING222010004) and InES—Ciencia—Abierta (INCA210005).

**Data Availability Statement:** Data are contained within the article.

**Conflicts of Interest:** The authors declare no conflict of interest.

## References

1. FEMA. *State of the Art Report on Connection Performance*; SAC Joint Venture; FEMA: Washington, DC, USA, 2000.
2. AISC. *AISC 358—Prequalified Connections for Special and Intermediate Steel Moment Frames for Seismic Applications*; American Institute of Steel Construction: Chicago, IL, USA, 2005.
3. Horikawa, K.; Sakino, Y. Damages to Steel Structures Caused by the 1995 Kobe Earthquake. *Struct. Eng. Int.* **1996**, *6*, 181–182. [CrossRef]
4. Nakashima, M.; Roeder, C.W.; Maruoka, Y. Steel Moment Frames for Earthquakes in United States and Japan. *J. Struct. Eng.* **2000**, *126*, 861–868. [CrossRef]
5. Whittaker, A.; Moehle, J.; Higashino, M. Evolution of seismic building design practice in Japan. *Struct. Des. Tall Build.* **1998**, *7*, 93–111. [CrossRef]
6. Nakashima, M.; Inoue, K.; Tada, M. Classification of damage to steel buildings observed in the 1995 Hyogoken-Nanbu earthquake. *Eng. Struct.* **1998**, *20*, 271–281. [CrossRef]
7. Chen, C.-C.; Lin, C.-C. Seismic performance of steel beam-to-column moment connections with tapered beam flanges. *Eng. Struct.* **2013**, *48*, 588–601. [CrossRef]
8. Kang, C.-H.; Kim, Y.-J.; Shin, K.-J.; Oh, Y.-S. Experimental Investigation of Composite Moment Connections with External Stiffeners. *Adv. Struct. Eng.* **2013**, *16*, 1683–1700. [CrossRef]
9. Schneider, S.P.; Teeraparbwong, I. Inelastic Behavior of Bolted Flange Plate Connections. *J. Struct. Eng.* **2002**, *128*, 492–500. [CrossRef]
10. Malley, J.O.; Carter, C.J.; Saunders, C.M. Seismic Design Guidelines and Provisions for Steel-Framed Buildings. *Earthq. Spectra* **2000**, *16*, 179–203. [CrossRef]
11. Zhang, X.; Zheng, S.; Zhao, X. Seismic performance of steel beam-to-column moment connections with different structural forms. *J. Constr. Steel Res.* **2019**, *158*, 130–142. [CrossRef]
12. Morshedi, M.A.; Dolatshahi, K.M.; Maleki, S. Double reduced beam section connection. *J. Constr. Steel Res.* **2017**, *138*, 283–297. [CrossRef]
13. Vetr, M.; Miri, M.; Haddad, A. Seismic Behavior of a New Reduced Beam Section Connection by Drilled Holes Arrangement (RBS_DHA) on the Beam Flanges through Experimental Studies. In Proceedings of the 15th World Conference on Earthquake Engineering, Lisbon, Portugal, 24–28 September 2012.
14. Nuñez, E.; Torres, R.; Herrera, R. Numerical Study on Cyclic Response of End-Plate Biaxial Moment Connection in Box Columns. *Metals* **2017**, *25*, 523. [CrossRef]
15. Tao, Z.; Li, W.; Shi, B.-L.; Han, L.-H. Behaviour of bolted end-plate connections to concrete-filled steel columns. *J. Constr. Steel Res.* **2017**, *134*, 194–208. [CrossRef]
16. Astaneh-Asl, A. *Seismic Design of Steel Column-Tree Moment-Resisting Frames*; Departement of Civil and Environmental Engineering—University of California: Berkeley, CA, USA, 1997.
17. Baharmast, A.; Razzaghi, J.; Kamouneh, S. Modification of pre-Kobe column-tree moment resisting connection. *Asian J. Civ. Eng.* **2018**, *19*, 223–237. [CrossRef]
18. Gharebaghi, R.; Hosseini, A. Local behavior of column-tree connections with considering bolt-hole clearance and bolt pretension effects. *Int. J. Steel Struct.* **2017**, *17*, 379–388. [CrossRef]
19. Palizzolo, L.; Vazzano, S. Iterative Optimal Design of Special Moment Resisting Devices for Steel Frames. *IOP Conf. Ser. Mater. Sci. Eng.* **2021**, *1203*, 032079. [CrossRef]
20. Chen, Y.; Tong, L.; Chen, Y.; Zhou, X. Experimental study on cyclic behavior of cast steel connectors for beam-to-column joints. *Adv. Struct. Eng.* **2016**, *19*, 1677–1695. [CrossRef]
21. Yeow, T.Z.; Orumiyehei, A.; Sullivan, T.J.; MacRae, G.A.; Clifton, G.C.; Elwood, K.J. Seismic performance of steel friction connections considering direct-repair costs. *Bull. Earthq. Eng.* **2018**, *16*, 5963–5993. [CrossRef]
22. Oh, K.; Li, R.; Chen, L.; Hong, S.-B.; Lee, K. Cyclic testing of steel column-tree moment connections with weakened beam splices. *Int. J. Steel Struct.* **2014**, *14*, 471–478. [CrossRef]
23. AISC. *AISC 341—Seismic Provisions for Structural Steel Buildings*; American Institute of Steel Construction: Chicago, IL, USA, 2016.
24. Oh, K.; So, J.; Ha, H.; Lee, K. Seismic performance evaluation of Korean column-tree steel moment connections. *Int. J. Steel Struct.* **2016**, *16*, 1287–1298. [CrossRef]
25. Lin, X.; Chen, Y.; Yan, J.-B.; Hu, Y. Seismic Behavior of Welded Beam-to-Column Joints of High-Strength Steel-Moment Frame with Replaceable Damage-Control Fuses. *J. Struct. Eng.* **2020**, *146*, 04020143. [CrossRef]
26. Karami, B.; Hashemi, B.H.; Ramhormozian, S.; Zarabimanesh, Y. Numerical study on prequalification and cyclic performance of column-tree connections. *Structures* **2022**, *41*, 331–348. [CrossRef]

27. Kim, T.; Yu, E. Seismic analysis of steel moment frames with column-tree connections. *J. Constr. Steel Res.* **2020**, *168*, 105871. [CrossRef]
28. Akagwu, P.; Ali, F.; Nadjai, A. Behaviour of bolted steel splice connections under fire. *J. Constr. Steel Res.* **2020**, *170*, 106103. [CrossRef]
29. Saravanan, M.; Goswami, R.; Palani, G.S. Replaceable Fuses in Earthquake Resistant Steel Structures: A Review. *Int. J. Steel Struct.* **2018**, *18*, 868–879. [CrossRef]
30. AISC. *AISC 360—Specification for Structural Steel Buildings*; American Institute of Steel Construction: Chicago, IL, USA, 2016.
31. ANSYS Inc. *ANSYS 2022*; ANSYS Inc.: Canonsburg, PA, USA, 2022.
32. Vilela, P.M.L.; Carvalho, H.; Grilo, L.F.; Montenegro, P.A.; Calçada, R.B. Unitary model for the analysis of bolted connections using the finite element method. *Eng. Fail. Anal.* **2019**, *104*, 308–320. [CrossRef]
33. Nuñez, E.; Parraguez, G.; Herrera, R. Bidirectional Response of Weak-Axis End-plate Moment Connections: Numerical Approach. *Metals* **2020**, *10*, 964. [CrossRef]
34. Herrera, R.; Salas, C.; Beltran, J.F.; Nuñez, E. Experimental performance of double built-up T moment connections under cyclic loading. *J. Constr. Steel Res.* **2017**, *138*, 742–749. [CrossRef]
35. Grondin, G.; Jin, M.; Josi, G. *Slip Critical Connections—A Reliability Analysis for Design at the Ultimate Limit State*; University of Alberta: Edmonton, AB, Canada, 2007.
36. Maison, B.F.; Speicher, M.S.; Maison, M.B.F.; Eeri, M. Loading Protocols for ASCE 41 Backbone Curves. *Earthq. Spectra* **2016**, *32*, 2513–2532. [CrossRef]


**Disclaimer/Publisher's Note:** The statements, opinions and data contained in all publications are solely those of the individual author(s) and contributor(s) and not of MDPI and/or the editor(s). MDPI and/or the editor(s) disclaim responsibility for any injury to people or property resulting from any ideas, methods, instructions or products referred to in the content.